Available online at www.sciencedirect.com

SCIENCE DIRECT®

Journal of Molecular Catalysis A: Chemical 204–205 (2003) 27–53

JOURNAL OF MOLECULAR CATALYSIS A: CHEMICAL

www.elsevier.com/locate/molcata

Review

Approaches to design of active structures by attaching and molecular imprinting of metal complexes on oxide surfaces

Mizuki Tada, Yasuhiro Iwasawa*

Department of Chemistry, Graduate School of Science, The University of Tokyo, 7-3-1 Hongo, Bunkyo-ku, Tokyo 113-0033, Japan

Received 5 November 2002; received in revised form 28 February 2003; accepted 4 March 2003

Dedicated to Professor Renato Ugo on the occasion of his 65th birthday

Abstract

This paper attempts to review recent examples of chemical design of catalytically active metal-complexes on oxide surfaces by means of attaching and molecular imprinting techniques. Metal complexes formed on oxide surfaces have generally different structures from their homogeneous analogues and often exhibit remarkable reactivities and catalyses based on the unique structures. Recently, functionalized catalytic sites have been combined to attached metal complexes for design of molecular shape selective space regulating catalyses. Here, we pick up several recent interesting supported metal-complex catalysts with different metal units. We also introduce new design of catalytic sites achieved by combining two methods of metal-complex attaching and molecular imprinting on oxide surfaces.
© 2003 Elsevier B.V. All rights reserved.

Keywords: Catalyst design at oxide surface; Metal-complex attaching; Molecular imprinting; Template; Rhodium; Monomer; Dimer; Cluster; Hydrogenation; Dehydration; Hydroformylation; Ammoxidation; Hydroxyalkylation; Epoxidation

1. Introduction

Chemical design of enzymatic catalysts with high activity and molecular recognition has been a long-term challenge in many fields such as organic chemistry, organometallic chemistry, inorganic chemistry, and catalytic chemistry. Both catalytically active site and selective reaction space are necessary to regulate approach of reactant molecules to the active site and their structural change in the space. Natural enzymes realize such wonderful catalyses under mild reaction conditions, however, preparation of artificial enzyme catalysts as molecular architecture has generally been difficult and unaddressed challenges yet. On the other hand, natural enzymes have great disadvantageous such as limited application to only particular reactants, possible operation under limited reaction media and conditions, thermally unstability, high cost, etc.

Since the discovery of catalysis of metal complexes by Wilkinson and coworkers [1], many metal complexes have been used as catalytic active species in homogeneous systems and catalytic reaction mechanisms on metal complexes have been investigated for various reactions. It is well known that ligands coordinated to metal center significantly modify and regulate not only reactivity of the metal electronically but also space around the metal geometrically. As a result, sharp selectivity can be achieved on metal-complex catalysts, which may be difficult to obtain on metal

* Corresponding author. Tel.: +81-3-5841-4363; fax: +81-3-5800-6892.
E-mail address: iwasawa@chem.s.u-tokyo.ac.jp (Y. Iwasawa).

1381-1169/$ – see front matter © 2003 Elsevier B.V. All rights reserved.
doi:10.1016/S1381-1169(03)00284-X

particles and metal single crystal surfaces. Application of the regulation by ligands in metal complexes finds selective catalysis and asymmetric synthesis.

However, homogeneous metal complexes in solutions are generally easy to gather during catalytic cycles and to cause decomposition of metal complexes, resulting in loss of the catalytic activities. Transformation of homogeneous catalysts to heterogeneous catalysts with molecular-level active structures has been accomplished by attaching metal complexes on oxide or polymer supports [2–10]. The attached metal complexes may be further treated chemically at the surface, which provides unique structures different from their homogeneous analogues and often remarkable catalytic properties. Understanding and controlling catalyst surfaces are the key issues for development of new catalysts, but conventional supported metal catalysts are generally heterogeneous and complicated, whose characterizations are difficult especially under catalytic reaction conditions. Molecular-level control of catalyst surfaces is necessary for design of multi-functionalized catalytic sites.

The new and distinct materials and chemistry prepared stepwise in a controllable manner by using organometallic and inorganic complexes as precursors provide an opportunity for the development of efficient catalytic molecularly-organized surfaces. The key factors of chemical design of supported catalyst surfaces are composition, structure, oxidation state, distribution, morphology, polarity, etc. which should be organized at the surface. In the development of novel catalysts, new chemical concepts regarding composition or structure are conceived.

In this review, we attempt to summarize recent examples of chemical design of catalytic sites by the metal-complex attaching technique, their unique catalytic properties, and catalytic reaction mechanisms. Further, the article is devoted to progress in molecular imprinting as a new tool for design of shape-selective metal complexes at surfaces.

2. Tripodal polyphosphine rhodium catalysts on SiO_2 surface

Zwitterionic Rh(I) complexes (sulfos)Rh(cod) (**1**) and (sulfos)$Rh(CO)_2$ (**2**) [sulfos = $–O_3S(C_6H_4)CH_2C(CH_2PPh_3)$; cod = cycloocta-1,5-diene] are effective catalysts for hydrogenation, hydroformylation, and hydrogenolysis in mixture of water and organic media [11,12]. The Rh complex remaining polar phase can be recycled by separation, but the manipulation must be done under inert atmosphere. These complexes were heterogenized by controlled adsorption on partially dehydroxylated silica, and the obtained heterogeneous catalysts were more stable, more selective, and easier to recycle than the unsupported analogues [13].

Supporting onto a high surface area silica is performed by controlled adsorption of the sulfonate tail of sulfos to surface silanol groups via hydrogen bonding as monitored by IR, as shown in Fig. 1. The resulting

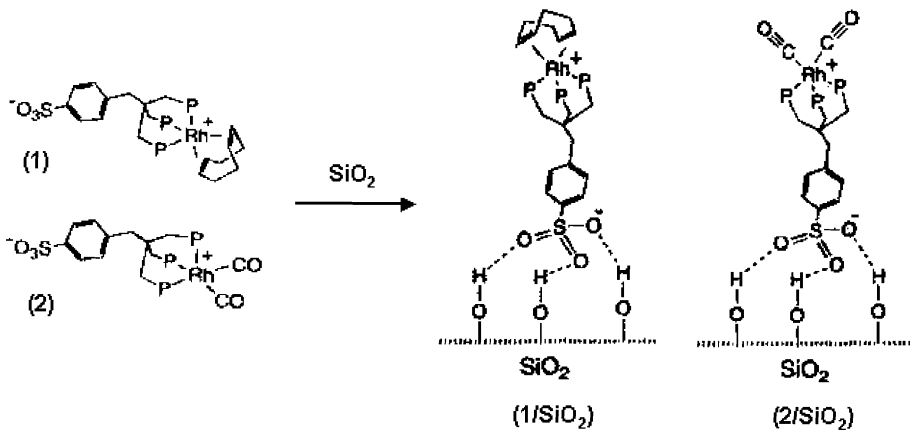

Fig. 1. SiO_2-supported Zwitterionic Rh-monomer catalysts via hydrogen bonding with their sulfos tails.

hydrogen bonding between the Rh complex and the surface is stable and the supported complexes are not extracted by repeated washing of CH_2Cl_2. Characterizations were performed by means of IR, NMR, EXAFS, and TPD. ν_{CO} bands in IR spectra and EXAFS analysis revealed two remarkable features, no perturbation of the Rh coordination sphere and monomeric dispersion of the Rh complexes on the surface. Variable-temperature ^{31}P NMR spectra showed that the Rh complex is five-coordinated structure closer to a square-pyramid than to a trigonal-bipyramid.

Suprisingly, two CO ligands on the supported Rh complex (**2**/SiO_2) were not lost by heating under O_2 atmosphere for 2.5 h at 393 K. The remarkable stability toward O_2 is contrasted to facile decomposition of **1**/SiO_2 with a cod ligand in comparable conditions. This different reactivities of **1**/SiO_2 and **2**/SiO_2 may reasonably be interpreted in terms of a stronger coordination of the CO ligands to Rh.

The supported Rh complex **1**/SiO_2 is active for catalytic alkene hydrogenation at 393 K in a flow system. No catalyst deactivation is observed after 15 h reaction. In general, organometallic catalysts with triphos ligand are converted to H-bridged Rh dimers under H_2 at high temperatures [14], resulting in decrease of the catalytic activity. Under H_2 ambient, **1**/SiO_2 looses the cod ligand to form hydride species, while the triphos P atoms remain at the distances of 0.226–0.234 nm as suggested by EXAFS. Further reaction with alkenes unchanged Rh–P bonds and formed Rh–C bonds. In all cases, there was no indication of the formation of contiguous Rh–Rh sites. It means that the catalytic active sites are isolated Rh monomers at the surface. In contrast, under hydroformylation conditions with a mixture of H_2, CO, and alkene, no hydroformylated product was observed and **1**/SiO_2 was converted to the dicarbonyl derivative **2**/SiO_2 completely. The dicarbonyl species was too stable and inactive for solid–gas hydrogenation reactions.

In contrast to solid–gas reactions, the Rh complexes are active for both hydrogenation and hydroformylation in liquid-phase conditions. **1**/SiO_2 catalyzed hydrogenation of styrene to ethylbenzene and hydroformylation of 1-hexene with a little hydrogenation product (3.5%). CO coordination to the Rh center is much faster than hydride migration. Furthermore, the catalytic reactions proceeded without any leaching of the supported Rh complexes and could be reused in both reactions, yielding unchanged conversions and product compositions. As compared to the homogeneous analogues **1** and **2**, the supported catalysts gave higher conversion and selectivity for corresponding aldehyde in the hydroformylation. Transformation of Rh monomer to Rh dimer has been proposed to be the issue responsible for decrease in activity of the homogeneous catalysts. Therefore, immobilization on the silica surface is an effective method to maintain the high catalytic activity of initial Rh complexes by isolation of the Rh sites. The difference of the hydroformylation activities between solid–gas and solid–liquid systems may be ascribed to cooperation of the solvent that assists to unfasten a part of the triphos arm.

3. Rh dimers attached on inorganic oxide surfaces for hydroformylation

Ethene hydroformylation on supported Rh particle catalysts shows a maximum activity with on optimum particle size, suggesting contribution of metal ensembles with Rh–Rh bonding to the catalytic performance, while in homogeneous systems mononuclear Rh complexes catalyze the reaction. There is a clear contrast. Demonstration of role of metal–metal bondings for catalyses is one of the crucial issues for design of new catalytically active sites. In order to prepare supported metal species with metal–metal bond, there have been many attempts to attach di- and multi-nuclear metal complexes on oxide surfaces [2,4].

Supported Rh dimers were prepared by reaction of *trans*-[$(RhCp^*CH_3)_2(\mu\text{-}CH_2)_2$] ($Cp^*$ = pentamethylcyclopentadienyl) dimer with surface OH groups of SiO_2, TiO_2, Al_2O_3, and MgO [15]. Each step for the transformation at the surfaces was characterized by FT-IR and EXAFS [16]. On SiO_2 and TiO_2 surfaces, the Rh species are converted to Rh dimers with Rh–Rh bond as shown in Figs. 2 and 3. On the other hand, mononuclear species is formed on Al_2O_3 and the Rh complex decomposes on MgO (Fig. 3).

Catalytic activities and selectivities for ethene hydroformylation are summarized in Table 1. Compared with a conventional impregnated Rh catalyst, the Rh dimer on silica surface Rh_2/SiO_2 (**3**) shows high activity and selectivity. The Rh_2/SiO_2 (**3**) can be employed as an efficient catalyst in the gas phase hydroformylation, which is different from almost

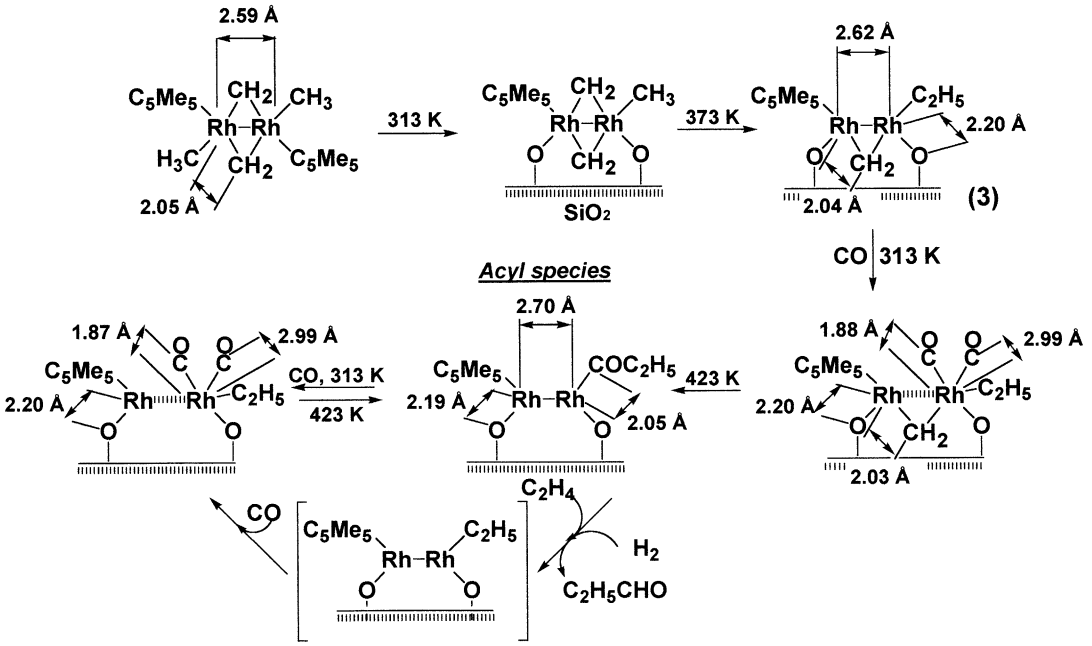

Fig. 2. Preparation of the Rh-dimer catalyst attached on a SiO_2 surface and its structural change during ethene hydroformylation.

inactive performance of Rh monomers on SiO_2. On the other hand, the other catalysts including Rh dimer on TiO_2 in Table 1 are inactive.

The Rh species and dynamic mechanism during the ethene hydroformylation on SiO_2 were characterized by FT-IR and EXAFS as shown in Fig. 2. A CO ligand reacts with an ethyl ligand coordinated to Rh to form an acyl ligand. The acyl is hydrogenated to the corresponding aldehyde. CO molecules coordinate to Rh again, while Rh–Rh bonding is broken, leading to two mononuclear sites (Fig. 2). The mononuclear species are transformed to the acyl species again at 423 K, accompanied with rebonding of Rh–Rh. The transformations between these structures are reversible, which provides a catalytic cycle for the ethene hydroformylation. Note that the catalytic ethene hydroformylation

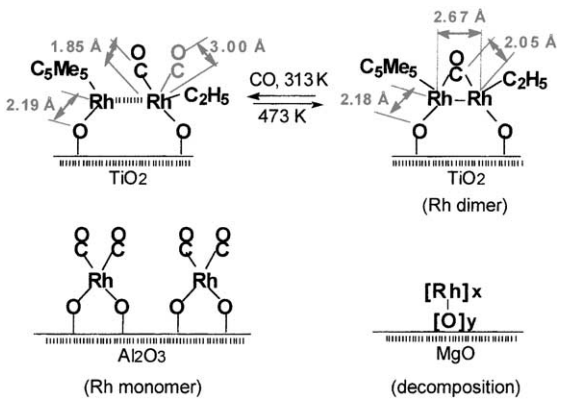

Fig. 3. Supported Rh catalysts on TiO_2 (dimer), Al_2O_3 (monomer), and MgO (metal ensemble). Acyl species was not formed on the TiO_2-supported Rh dimer.

Table 1
Catalytic activities and selectivities for ethene hydroformylation on the Rh-dimers attached on SiO_2, TiO_2, Al_2O_3, and MgO at 413 K[a]

Catalyst	TOF (total)	TOF (ethene)	TOF (propanal)	Selectivity (%)
Impregnated Rh/SiO_2	22.8	21.5	1.3	5.6
Rh_2/SiO_2	36.9	4.1	32.8	88.9
Rh_2/TiO_2	6.3	6.3	0	0
Rh/Al_2O_3	6.8	6.8	0	0
Rh_x/MgO	56.0	56.0	0	0

TOF: 10^{-4} min^{-1}.
[a] $CO:H_2:C_2H_4$ = 1:1:1 (total pressure = 40.0 kPa).

on Rh_2/SiO_2 (**3**) proceeds in conjunction with breaking and rebonding of Rh–Rh bond. This is the first example which clearly illustrates how the metal–metal bonding plays an essential role in catalysis. In the Rh dimer (**3**), one Rh atom with the acyl ligand works as the reaction site, while another Rh atom promotes the Rh reaction site for the CO insertion.

In spite of dimer structures of Rh_2/SiO_2 and Rh_2/TiO_2, their reactivities are much different from each other. The dimer structure of Rh_2/TiO_2 did not act as a catalytic site for ethene hydroformylation, where a CO-bridged Rh dimer structure was formed at 473 K as shown in Fig. 3. Further CO treatment brought about dissociation of the Rh–Rh bond to mononuclear species, but acyl species as a key intermediate for the hydroformylation was not formed at the reaction temperature. The difference may be caused by electronic and geometric states of the Rh sites.

Hydroformylation reaction of alkenes is known to proceed on mono-metal site like mononuclear metal complexes in homogeneous systems. However, mono-metal sites are generally disadvantageous because of necessity to eliminate a part of intimate ligands to form an unsaturated species. On the other hand, on the attached Rh dimer, it is not necessary to dissociate any ligands during the catalytic cycle, and hence the Rh dimer acts as effective catalytic site. Chemistry of the Rh dimer is different from chemistry of the homogeneous Rh monomer. CO insertion to alkyl on the Rh monomer proceeds only in the presence of excess CO and acyl decomposes to CO and alkyl under vacuum. In contrast, CO insertion proceeds under vacuum without excess CO and acyl decomposes in the presence of CO. The catalytic ethene hydroformylation on Rh_2/SiO_2 (**3**) is referred to metal-assisted catalysis by the two adjacent Rh atoms.

4. Nb monomer, dimer, and monolayer on SiO_2 surfaces

Niobium has been considered to be a poor element as a catalyst, but SiO_2-attached Nb species prepared stepwise in a controllable manner acts as an effective catalyst for ethanol oxidation [17]. Three types of Nb species, monomer, dimer, and monolayer can be prepared on SiO_2 surfaces by use of different Nb precursors. They exhibited unique catalytic behaviors attended to their Nb structures [5,18]. The design of Nb structures on SiO_2 surfaces is a representative document of the structure-catalytic function relationship in a molecular level.

The SiO_2-attached Nb monomer catalyst (**4**) was prepared by the use of $Nb(\eta^3\text{-}C_3H_5)_4$ as precursor and characterized by EXAFS, FT-IR, Raman, ESR, and XPS. $Nb(\eta^3\text{-}C_3H_5)_4$ was reacted with surface OH groups of SiO_2, followed by stepwise treatments with H_2 and O_2. Resultant Nb structure was a four-O-coordinated monomer and Nb–O and Nb–Si interatomic distances were determined to be 0.168, 0.193, and 0.326 nm, respectively, as shown in Fig. 4. No Nb–Nb bonding is observed by EXAFS, demonstrating that the Nb^{5+} ions are distributed as monomers on the SiO_2 surface.

Nb dimers on SiO_2 (**5**) in Fig. 4 can also be prepared by using a dimeric Nb precursor $[Nb(\eta^5\text{-}C_5H_5)_4H\text{-}\mu\text{-}(\eta^5,\ \eta^1\text{-}C_5H_4)]_2$ in controllable steps [12]. The first step of preparation of (**5**) was the reaction of the hydride ligand with surface silanols at 313 K to form surface-attached Nb dimers with Nb–Nb, Nb–C, and Nb–O (surface) at the bond distances of 0.334, 0.243, and 0.201 nm, respectively.

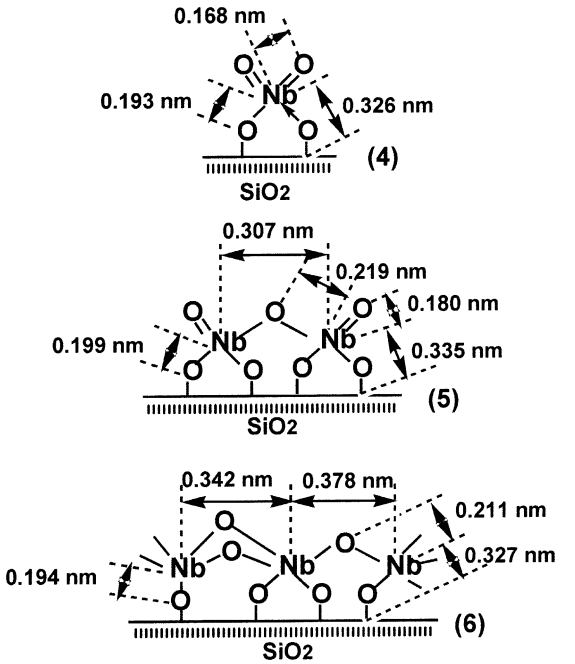

Fig. 4. Structures of the Nb monomer (**4**), dimer (**5**), and monolayer (**6**) attached on SiO_2 surface.

Table 2
Catalytic performances of the Nb monomer, dimer, and monolayer supported on SiO_2, and an impregnated Nb catalyst for dehydrogenation and dehydration of ethanol[a]

Catalyst	Total	Initial rate		Selectivity (%)		
		AA	E + DE	AA	E	DE
Monomer (**4**)[b]	1.25	1.20	0.049	96.1	2.8	1.1
Dimer (**5**)[b]	0.18	0.004	0.176	2.1	24.2	73.7
Monolayer (**6**)[c]	0.11	0.001	0.106	0.9	99.1	0.0
Impregnated[b]	0.17	0.052	0.118	30.5	20.2	49.3

Initial rate: mmol min^{-1} (g Nb)$^{-1}$.
[a] AA: acetaldehyde, E: ethene, DE: diethyl ether, ethanol: 3.1 kPa.
[b] Temperature: 523 K.
[c] Temperature: 573 K.

Then the obtained surface dimers were converted to the Nb dimer catalyst (**5**) by stepwise treatments with H_2 and O_2 at 773 K. The oxygen-bridged surface Nb dimers (**5**) with a Nb–Nb distance of 0.307 nm (coordination number: 0.9) were chemically bound to the SiO_2 surface at a Nb–Si interatomic distance of 0.335 nm through the interfacial Nb–O (surface) bond at 0.199 nm as shown in Fig. 4.

Further, Nb-oxide monolayers on SiO_2 (**6**) in Fig. 4 was successfully prepared by using $Nb(OC_2H_5)_5$ as a precursor [5]. The Nb monolayer growth was monitored mainly by Nb–Si bond (0.327 nm) formation characterized by EXAFS. In the monolayer structure (**6**), there are two different Nb–Nb separations at 0.342 and 0.378 nm, both being considered to have one or two bridging oxygens (Nb–O: 0.211 nm). The interfacial Nb–O bonds are similar to those of the other Nb structures (**4** and **5**).

The Nb catalysts exhibit different catalytic behaviors for ethanol as shown in Table 2. The Nb monomer (**4**) acts as an effective catalyst for the dehydrogenation of ethanol to acetaldehyde and H_2 in the temperature range 423–523 K. The activity is much higher than that of a usual impregnation Nb catalyst and the selectivity is as high as 95–100%. Ethanol dissociates on the Nb monomer to form Nb-ethoxide species (**7**), but the Nb-ethoxide intermediate is very stable and never decomposes until 600 K. Above 600 K, the Nb-ethoxide species is "dehydrated" to ethene and water as shown in Fig. 5. On the other hand, when the Nb-ethoxide intermediate is exposed to ethanol, the ethanol dehydrogenation proceeds at much lower temperatures such as 423 K, with ca. 100% selectivity. Note that the reaction path was switched over from dehydration (γ–CH bond break) to dehydrogenation (β–CH bond break) by the second ethanol molecule weakly adsorbed on the Nb-ethoxide (**8**). Even if an adsorbed species at the surface is too stable in vacuum or before catalysis, the catalytic reaction is able to proceed through the same species by activation of the intermediate by the reactant [6,19]. Thus, it may be critical for the dehydrogenation on the Nb sites to create a vacant site with an appropriate conformation for the transition state on which electron donation-induced activation of β-hydrogen of the ethoxy group is favorable.

The reactivity of Nb dimer (**5**) is entirely different from that of the Nb monomer, where diethyl ether is mainly produced in Table 2. The dehydration on the Nb dimer (**5**) was independent of the presence or absence of the ambient ethanol. The dehydrogenation observed on the Nb monomer (**4**) was remarkably suppressed to 1/300 and the dehydration was promoted four times on the dimer (**5**), indicating that the Nb dimers on SiO_2 have an acidic character. It is to be noted that the change in the number of Nb atoms at the active sites from one to two metals gives rise to

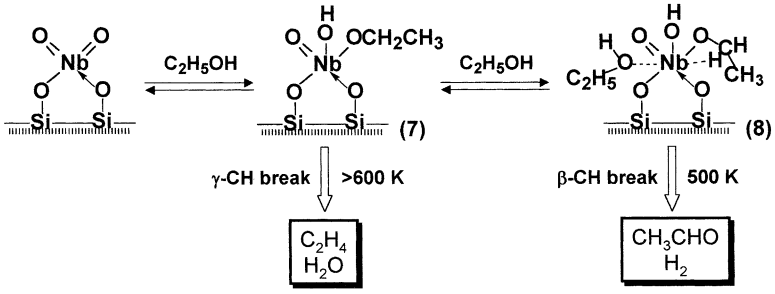

Fig. 5. Unique reactivity of the supported Nb monomer catalyst to ethanol.

a complete reverse of basicity/acidity in the catalytic properties. In the dimer (**5**), the access of a second ethanol molecule to the Nb atom coordinated with a first ethanol molecule in a preferable conformation is difficult unlike the case of the monomer (**4**). Furthermore, the Lewis acidity of the Nb atoms in the dimer (**5**) is increased by oxygen bridge.

The monolayer (**6**) is active and selective for ethene formation from ethanol in the temperature range 423–573 K as shown in Table 2. The monolayer catalyst (**6**) is selective for the intramolecular dehydration of ethanol to ethane, suggesting that the Lewis acid sites in the monolayer niobium oxides (**6**) may be distributed in an isolated manner. The niobium oxide layer is somewhat distorted by a structural mismatch between the Nb oxide overlayer and the SiO_2 surface lattice as proved by EXAFS. The distortion and mismatch should be released by the creation of defects, resulting in Lewis-acidic Nb sites. Nb oxide overlayers on various supports have been extensively investigated and characterized by Raman spectroscopy [20]. These structures are described as being made up of an octahedrally coordinated NbO_6 structure with different degree of distortion. The Lewis acid sites may be dispersed basically at the NbO_6 overlayer. This type of catalyst may be applicable to intramolecular dehydration processes in organic synthesis, sugar conversion, natural products synthesis, etc.

5. Ir_4 cluster on Al_2O_3 and MgO

As shown in the preceding sections, metal species exhibit various catalytic activities based on their structures. Especially, metal clusters composed of plural metal sites have interactions between metal atoms, which give unique reactivity not to be observed on mononuclear metal atoms [15,21,22]. Further in the case of oxide-supported metal clusters, reactivity is influenced by both oxide supports and ligands. Chemical bonding between oxide surface and supported metal clusters changes electronic state of the metal sites and coordinated ligands also dominate coordination of reactant molecules on the metals.

Metal surfaces, for examples, Pt, Pd, and Rh, etc. easily hydrogenate alkenes to corresponding alkanes. Understanding role of metal–metal interaction and mechanism of hydrogenation on metal sites is very important. However, metal particles that are models of such metal–metal interactions are difficult to characterize because of their various kinds of metal sites. Metal clusters with uniform metal ensembles are used as model of such metal catalysts to investigate mechanistic aspects of their catalyses.

Table 3
Catalytic activities of the supported Ir_4 catalysts for hydrogenation of propene and ethene[a]

Catalyst	Reactant	TOF (s^{-1})
Ir_4/γ-Al_2O_3	Propene	0.21
Ir_4/MgO	Propene	0.091
Ir_4/γ-Al_2O_3	Ethene	0.23
Ir_4/MgO	Ethene	0.052

[a] Temperature: 295 K, p_{H_2} = 13.3 kPa, p_{alkene} = 5.3 kPa, p_{He} = 82.2 kPa.

Ir_4 clusters on Al_2O_3 and MgO act as hydrogenation catalysts for ethene and propene [23–26]. These catalysts were prepared by decarbonylation of $[Ir_4(CO)_{12}]$ on porous γ-Al_2O_3 or of $[HIr_4(CO)_{11}]^-$ on MgO, respectively. Conventional measurements of catalytic reaction rates were complemented by EXAFS and IR spectroscopies to determine the structure of Ir_4 clusters and adsorbed molecules, and then identify catalytic intermediates on the Ir_4. Catalytic activity of Ir_4/γ-Al_2O_3 was significantly greater than that of Ir_4/MgO (Table 3).

During the reaction with H_2 or/and ethene and propene at 240–298 K, Ir–Ir coordination numbers estimated by EXAFS analyses remained close to 3 on both oxide supports, indicating that the supported Ir_4 clusters remained tetrahedral four-membered Ir cluster. The absence of higher Ir–Ir shell peaks in the spectra was consistent with the Ir_4 clusters being isolated on the surface. The two Ir–O distances of 0.21 and 0.26 nm suggested the coordination with oxide surfaces was polydentate form by surface oxygen and hydroxyl group.

The ligands on supported Ir_4 observed by IR spectroscopy during steady-state alkene hydrogenation included hydrocarbons not observed with the alkene alone. The ligands were identified by varying the reaction conditions and comparing against published spectra. For example, during ethene hydrogenation on Ir_4/γ-Al_2O_3 at 288 K and 101.3 kPa, four ethene-derived ligands were observed, ethyl (2921 and 2870 cm^{-1}), π-bonded ethene (3055 cm^{-1}),

ethylidyne (2890 cm^{-1}), and di-σ-bonded ethene (2988 cm^{-1}). With changing reaction conditions, the IR band intensities of some ligands changed, whereas others remained nearly constant.

A ligand is a reaction intermediate if its concentration can be correlated with the catalytic activity of the system. As partial pressure of H_2 (p_{H_2}) increased, the intensities of the IR bands representing π-bonded ethene, ethylidyne, and di-σ-bonded ethene on $Ir_4/\gamma\text{-}Al_2O_3$ remained nearly constant. On the other hand, the intensities of the ethyl bands increased almost proportionally with p_{H_2}, accompanied with the catalytic activity. Thus, the ethyl conformation is identified as a reaction intermediate under these conditions, whereas π-bonded ethene, ethylidyne, and di-σ-bonded ethene are either 'spectators' or involved in virtually equilibrated elementary steps in the catalytic cycle.

In case of propene hydrogenation at $p_{H_2} = 40$ kPa, variation of $p_{C_3H_6}$ caused the 1-propyl band intensities to vary, along with the catalytic reaction rate. The intensity of the π-bonded propene band also correlated with the rate, indicating that it also is a significant reaction intermediate. Hence, hydrogenation of propene on the supported Ir_4 is suggested to proceed via the two intermediates, π-bonded propene and propyl species illustrated in Fig. 6. The similarity of the results obtained for ethene hydrogenation and propene hydrogenation implies that the two reactions proceed by the similar mechanisms on supported Ir_4, as they do on metal surfaces [27].

EXAFS spectra complement IR spectra by showing how changes in the reactant-derived ligands influence the cluster frame and its interaction with the oxide supports. During catalysis, the Ir–Ir distance and the longer non-bonding Ir–$O_{support}$ distance exceeded the corresponding distances observed under non-catalytic conditions, 0.262–0.268 and 0.256–0.273 nm, respectively. These distances increased with increasing the catalytic activity. Furthermore, the Ir–Ir distance increased with the IR bad intensities of ethyl on Ir_4, suggesting that ethyl ligands weaken the bonding within the tetrahedral Ir_4 cluster and cause the changes in the cluster framework and cluster/support interaction.

MgO and $\gamma\text{-}Al_2O_3$ differ in their electron-donor characteristics, and thus in their effects on the interaction of the clusters with reactant-derived ligands. The strongly basic MgO surface increased the charge density on Ir_4 more than the less basic $\gamma\text{-}Al_2O_3$ does, and consequently MgO reduces the strength of the

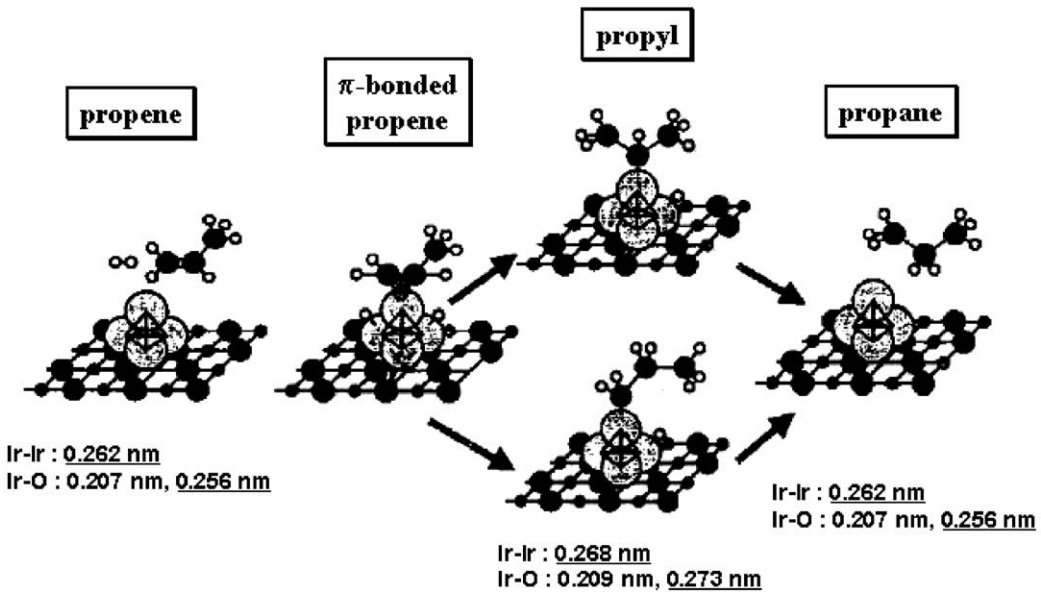

Fig. 6. Schematic representation of the hydrogenation of propene on Ir_4/MgO. Propene was initially adsorbed with π-bonded form on the Ir_4 cluster, then hydrogenated to give propyl species, which are hydrogenated to give propane. The Ir–Ir backbone and longer Ir–O bondings extended by the reaction with propene from 0.262 and 0.256 to 0.268 and 0.273 nm, respectively.

alkene-cluster interaction and thereby the catalytic activity. This interplay between the support and the reactant-derived ligands, whereby each influences the interaction of the metal cluster with the other, shows that the catalytic properties of supported metal catalysts can be tuned by careful choice of their supports.

6. Ammonia-promoted Re_6-cluster formation in H-ZSM-5 for selective oxidation/ammoxidation of propene

Rhenium is one of the oxophilic atoms effective to oxidation reactions [28]. ReO_x species are likely to have chemical interaction with various oxide supports and to exhibit unique catalytic properties which can not be observed on single rhenium oxides [29,30]. For example, ReO_x on Fe_2O_3 behave as a highly selective catalyst for oxidation–dehydration of methanol to methylal [31,32]. Very recently, new six-membered octahedral Re cluster in zeolite pores (H-ZSM-5 (HZ)) was found to be produced in situ under propene oxidation/ammoxidation in the presence of ammonia [33,34].

The Re/HZ catalyst was prepared by following procedure. Methyl trioxorhenium (MTO) was sublimed under vacuum at 333 K and the vapor was allowed to enter the chamber, where the zeolites were pretreated in situ at 673 K under vacuum. After the chemical vapor deposition (CVD) into zeolite pores, undeposited MTO was removed by evacuation at RT. The catalyst was treated at 673 K in He before use as a catalyst. For comparison, other two catalysts were also prepared by incipient wetness impregnation of NH_4ReO_4 and a physical mixing of NH_4ReO_4 and HZ.

The CVD catalyst exhibited good catalytic performance for the selectiveoxidation/ammoxidation of propene as shown in Table 4. Propene is converted selectively to acrolein (major) and acrylonitrile (minor) in the presence of NH_3 on the CVD catalyst, whereas cracking and complete oxidation to CO_2 proceed in the absence of NH_3. The difference is obvious. HZ had no catalytic activity for oxidation/ammoxidation of propene. Note that NH_3 opened a reaction path to convert propene to acrolein. The catalysts prepared by the impregnation and physical mixing methods catalyze the oxidation/ammoxidation but the selectivity is much lower than that for the CVD catalyst.

Table 4
Performances of supported ReO_x catalysts for selective oxidation/ammoxidation of propene at 673 K[a]

	HZ	Re/HZ in the presence of NH_3	Re/HZ in the absence of NH_3[b]
Conversion (%)	19.6	15.6	3.8
Cracking	93.2	5.5	31.8
Ethene	21.5	0.0	18.0
Methylamine	15.0	1.6	0.0
Dimethylamine	14.8	1.3	0.0
Ethylamine	22.0	2.6	0.0
Butene	19.9	0.0	13.8
Oxidation/ammoxidation	0.0	80.3	0.0
Acrolein	0.0	61.6	0.0
Acrylonitrile	0.0	18.7	0.0
Other products	6.8	14.2	68.2
Acetonitrile	0.0	4.6	4.0
CO_2	2.0	4.9	60.0
BTX	4.8	4.7	4.2

[a] Reaction conditions: GHSV 19,200 h^{-1}, $C_3H_6/NH_3/O_2/He = 7.5/7.5/10.0/75.0\%$.
[b] The reaction was conducted in the absence of NH_3 ($C_3H_6/O_2/He = 7.5/10.0/82.5\%$).

To investigate active Re species and the promoting role of NH_3, characterizations of the CVD catalyst have been performed by means of XRD, ^{29}Si and ^{27}Al solid-state MAS NMR, XANES, and EXAFS at the sequential stages for the reaction. XRD peak intensities decrease after loading of Re, which suggests a decrease in the ratio of Si/Al of the ZSM-5 framework and a little loss of the zeolite crystallinity during the catalyst preparation. As the result, the hydrophilic nature of HZ increases. Such changes were not observed for the other catalysts. Fig. 7 illustrates the structural changes of ReO_x species in the zeolite pore in the successive steps such as the MTO CVD, the He treatment at 673 K, the NH_3 treatment at 673 K, and the treatment with a mixture of propene and O_2 at 673 K. MTO adsorbs on a tetrahedral Al site and near a OH group in zeolite pores (**9**) at the first step. EXAFS analysis indicates the existence of two shells, Re–O (coordination number (CN) = 3.0, distance = 0.171 nm) and Re–C (CN = 1.1, distance = 0.201 nm), indicating retention of its original MTO structure. IR peak intensity at 3610 cm^{-1} attributed to zeolitic protons significantly decreases upon adsorption.

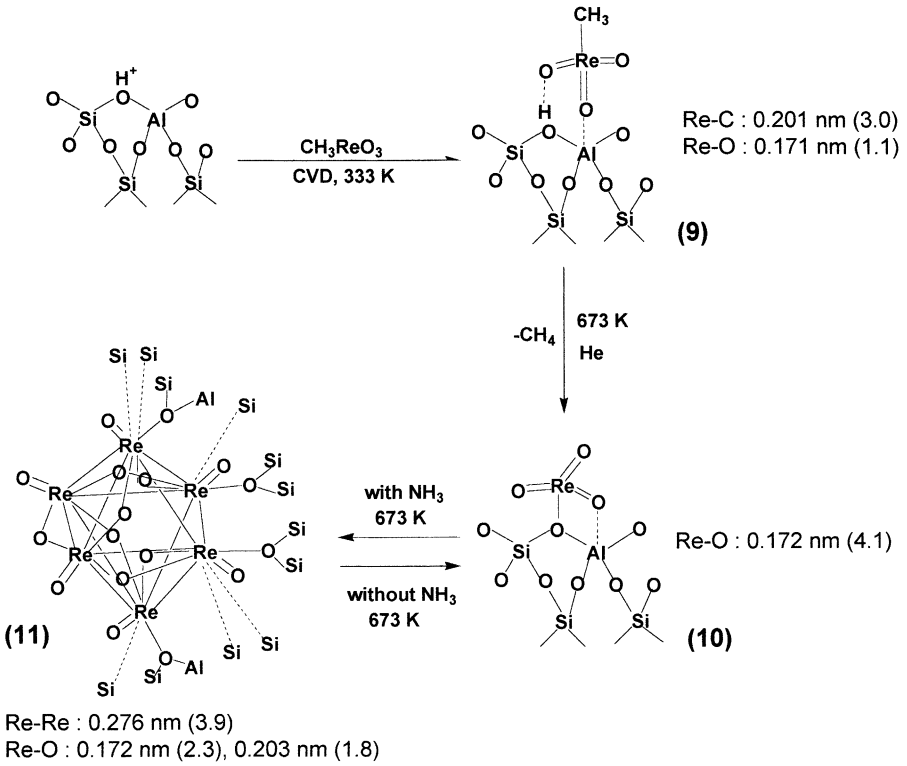

Fig. 7. A proposed structure of the active Re_6 cluster in the H-ZSM-5 pore channel with bond distances (coordination number). The Re_6 cluster is bound to pentagonal rings of the zeolite inner wall.

The adsorbed MTO in zeolite pore (**9**) decomposes at 673 K to form ReO_x species (**10**), evolving CH_4 (80% of Re quantity). Re L_1-edge XANES and L_3-edge EXAFS demonstrate that the Re species is mononuclear tetrahedral ReO_4 (Re–O = 0.172 nm) (**10**) as shown in Fig. 7. The bonding of hydrophilic [ReO_3] moiety to the Si–O–Al bridge-oxygen may increase hydrophilic nature of HZ as observed by XRD. Furthermore, chemical shift of tetrahedral Al species in ^{27}Al solid-state NMR changes from 60 ppm (**9**) to 50 ppm (**10**), indicating the additional bonding between [ReO_3] and tetrahedral Al site.

After NH_3 exposure, the XANES and EXAFS spectra changed remarkably and Re–Re bonding appeared. EXAFS data were well fitted by three shells, Re=O (CN = 2.3, distance = 0.172 nm), Re–O (CN = 1.8, distance = 0.203 nm), and Re–Re (CN = 3.9, distance = 0.276 nm). The coordination numbers of EXAFS analysis suggests the formation of a six-membered Re_6 cluster framework in octahedral geometry (**11**). Re atoms occupy six corners of the octahedron and each Re atom has four-coordinated with neighboring Re atoms, which agrees with the EXAFS analysis. The Re_6 clusters are supposed to be active species for the oxidation/ammoxidation of propene. Accompanied with the change of Re framework by the NH_3 exposure, the shifted MAS NMR signal for tetrahedral Al moves back to the original position at 60 ppm, indicating that the additional interaction between MTO and tetrahedral Al disappears by the NH_3 exposure.

The Re_6 cluster (**11**) with terminal and bridged oxygen atoms acts as catalytic site for selective propene oxidation under a mixture of propene, O_2 and NH_3. When the Re_6 catalyst is treated with propene and O_2 at 673 K, a further structural change occurs and the cluster is transformed back to the original [ReO_4] monomers (**10**) (Re–O: CN = 3.9, distance = 0.173 nm) reversibly. That is the reason why the catalytic activity is lost in the absence of ammonia.

7. Asymmetric catalyses by oxide-supported metal-complex catalysts

Catalytic asymmetric synthesis which needs fine regulation of catalytic sites is one of the most difficult subjects in catalytic chemistry. In the past decade, many chiral ligands were synthesized and applied to organic reactions such as hydrogenation, hydroformylation, epoxidation, etc. However, such chiral metal-complex catalysts are generally employed in homogeneous systems, where they often decompose or aggregate to metal ensembles. Heterogenization by attaching such metal complexes on oxide supports is one of the effective ways to solve these problems. However, the application of asymmetric metal complexes with chiral ligands to heterogeneous catalysts is not so easy. It is difficult to realize both high activity and high enantioselectivity because restriction of reaction space around the metal center to increase enantioselectivity results in a decrease of the catalytic activity. Especially, there are few reports of asymmetric metal-complexes on oxide surfaces that are stable for organic reagents and under severe catalytic conditions. In this chapter, we introduce two recent works for oxide-supported metal-complex catalysts for asymmetric epoxidation and hydroxyalkylation.

7.1. Silica-supported Ta catalysts for asymmetric epoxidations of allyl alcohols

Asymmetric epoxidation of allyl alcohols is an important reaction in synthetic organic chemistry. Homogeneous Ti complex with tartrate ligand have been used for the asymmetric epoxidation in industrial processes, but heterogeneous catalyst is more advantageous for the reaction because the epoxide product decomposes during its separation and the product separation is not necessary in heterogeneous catalyst systems.

Several oxide-supported Ti catalysts were prepared, any effective asymmetric catalyst was not reported yet. The chiral Ti complex with tartrate ligand forms peroxide complex with *tert*-butyl hydroperoxide and then coordinates with allyl alcohol. The intermediate takes a lot of coordinations with the chiral ligand, peroxide, and reactant, as shown in Fig. 8. If the chiral Ti complex is supported on SiO_2 by reaction with surface oxygen atoms, it can not accommodate all the ligands

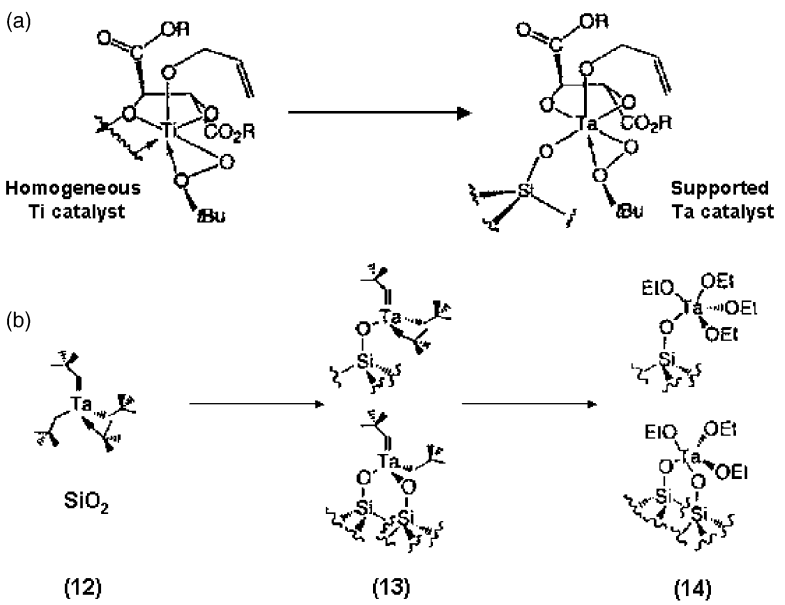

Fig. 8. (a) Coordination sphere of Ti-tartrate active in asymmetric epoxidations of allyl alcohols and hypothetical coordination sphere of Ta attached on SiO_2; (b) preparation procedure of the SiO_2-supported Ta catalysts.

Table 5
Asymmetric epoxidation of allyl alcohols on the Ta catalysts and their Ti analogues

Run	Catalyst	Reactant	Conversion (%)	Yield (%)	ee (%)
a	$Ti(OiPr)_4$	2-Propen-1-ol	76	72	80 (*S*)
b	Ti/SiO_2	2-Propen-1-ol	17	14	−9 (ca.) (*R*)
c	$Ta(OEt)_5$	2-Propen-1-ol	0.5 (ca.)	0.4	−45 (*R*)
d	**12**	2-Propen-1-ol	31	30	84 (*S*)
e	**12**	2-Propen-1-ol	30	29	−83 (*R*)
f	**13**	2-Propen-1-ol	60	56	85 (*S*)
g	**14**	2-Propen-1-ol	20	19.5	94 (*S*)
h	**13**	2-Hexen-1-ol	35	34	89 (*S*, *S*)
i	**13**, recycled	2-Hexen-1-ol	35	31	93 (*S*, *S*)

Metal/alcohol (molar ratio): a, b (5/100); c–g (2/100); h, i (4/100).

in its coordination sphere. In order to solve this problem, tantalum that can coordinate all the ligands at the same time was attached to SiO_2. The supported complexes were active for the catalytic asymmetric epoxidation of allyl alcohols [35].

SiO_2-supported Ta catalysts were prepared by attaching $Ta(=CHC(CH_3)_3)(CH_2C(CH_3)_3)$ on partially dehydroxylated silica as shown in Fig. 8. Two attached Ta species, monodentate and bidentate forms are obtained (**13**) [36]. Then, the supported Ta complexes were treated with ethanol to substitute alkyl and alkylidene ligands with ethoxy ligands (**14**). Ti analog of the supported Ta catalyst was also prepared from the silica and $Ti(OiPr)_4$ in the similar manner in order to compare catalytic behaviors of both catalysts.

Table 5 presents catalytic activities for asymmetric epoxidation of 2-propene-1-ol and trans-2-hexene-1-ol on the Ti and Ta catalysts. The reactions were conducted in the presence of diisopropyl tartrate (DIPT) for 48 h. The homogeneous $Ti(OiPr)_4$ are active and enantioselective for epoxidation of 2-propen-1-ol to (*S*)-glycidol (Table 6 (Run a)). But the supported Ti catalyst (Run b) shows poor activity and low selectivity under the identical condition. On the other hand, the supported Ta catalysts (**12**–**14**) exhibit good activity and enantioselectivity ((*S*)-glycidol) as shown in Table 5 (Runs d, f, and g), whereas homogeneous $Ta(OEt)_5$ gives (*R*)-glycidol with poor yield and ee (Table 5 (Run c)). As expected, the similar activity and enantioselectivity for (*R*)-glycidol is obtained with the catalyst (**12**) and the opposite tartrate (-)-DIPT (Run e). Leaching of the Ta complexes is not detected, demonstrating that the activities of the supported catalysts (**12**–**14**) are due to surface sites.

The catalysts also show good activities and enantioselectivities for the epoxidation of trans-2-hexen-1-ol. The solid washed with CH_2Cl_2 after the catalytic reaction can be reused without the addition of tartrate ligands, implying high stability of the supported Ta species.

The supported Ta catalysts are easily separated from the reaction medium and can be recycled without any loss of the catalytic activity and enantioselectivity in spite of poor activity of the Ta complex dissolved in solution. The activity and selectivity are similar level to those of the Ti-tartrate complex reported by Sharpless and coworkers [37,38]. The activity of supported Ta complex may result from the presence of well dispersed monomeric Ta site on the surface. The molecular Ta alkoxides in weakly polar solvents are tended to gather to dimers, which are poor active sites compared to the supported monomeric species. Further, chemical bonding between the monomeric Ta complex and the surface would also provide an activation of the catalytic site.

Table 6
Enantioselective Friedel–Crafts alkylation of 1,3-dimethoxybenzene on the Cu catalysts[a]

Catalyst	Conversion (%)	Selectivity (%)[b]	ee (%)
Homogeneous analog	44	94	72
15/SiO_2 (fresh)	72	90	92
15/MCM-41 (fresh)	77	98	82
15/MCM-41 (reuse)	73	94	84

[a] Performed at room temperature in acetonitrile by using 10% of heterogeneous catalysts, 0.5 mmol of 1,3-dimethoxybenzene and 0.6 mmol of methyl 3,3,3-trifluoropyruvate.
[b] Selectivity towards the hydroxyalkylation.

7.2. Immobilized chiral copper bisoxazoline for Friedel–Crafts hydroxyalkylation

Another general way to transform a homogeneous catalytic reaction into a heterogeneous process is coordination of the active metal complex to ligands that are anchored to a support. Anchoring the active catalytic center on a support with large surface area would help to overcome a problem that the activity decreases generally when homogenous catalysts are supported on inorganic supports due to inefficient interfacial mass transfer between the liquid phase and the solid. This general methodology has been successfully applied to non-stereoselective reactions. However, by anchoring a homogeneous enantioselective catalyst on an oxide support, the enantioselectivity would decrease dramatically compared with those obtained in solutions.

Immobilization of bisoxazolines that favor to coordinate with copper is an effective way to anchor Cu complexes. These ligands have been chemically bound various supports, such as soluble polymers, silica, mesoporous silica, clays, and zeolites. Very recently, chiral bisoxazoline copper complexes (**15**) anchored to silica and MCM-41 were reported as active and enantioselective catalysts for Friedel–Crafts hydroxyalkylation of 1,3-dimethoxybenzene with 3,3,3-trifluoropyruvate [39]. The enantiomeric excess (ee) values are even higher than those obtained for the unsupported complex in solution.

Preparation of the immobilized Cu-bisoxazoline catalyst (**15**) was accomplished by anchoring a copper bisoxazoline complex to 3-mercaptopropyl silanized surface using azoisobutyronitile (AIBN) as radical generator as shown in Fig. 9. Cu precursor was synthesized from copper triflate and the corresponding bisoxazoline ligand. Free OH groups on the surfaces were consumed by reaction with hexamethyldisilazane in order to prevent the Cu complex from decomposing on the surface. Adjustment of density of the complex on the surfaces is important to avoid undesirable association of the complexes and resulting in decrease of the enantioselectivity.

The catalytic activities of the immobilized Cu complexes in Table 6 are the highest values ever reported for Fridel-Crafts enantioselective reactions using metallic complexes anchored on SiO_2. Enantioselectivities increase up to about 92% after the immobilization. The ee values for the reaction are higher than that for the unsupported Cu complex as shown in Table 6. The lower ee values of MCM-41 than that of amorphous silica may be due to residual free OH groups. It is necessary for satisfaction of high enantioselectivity to control all the active sites in a desirable manner. No leaching of the copper ions occurs, and the heterogeneous catalyst can be

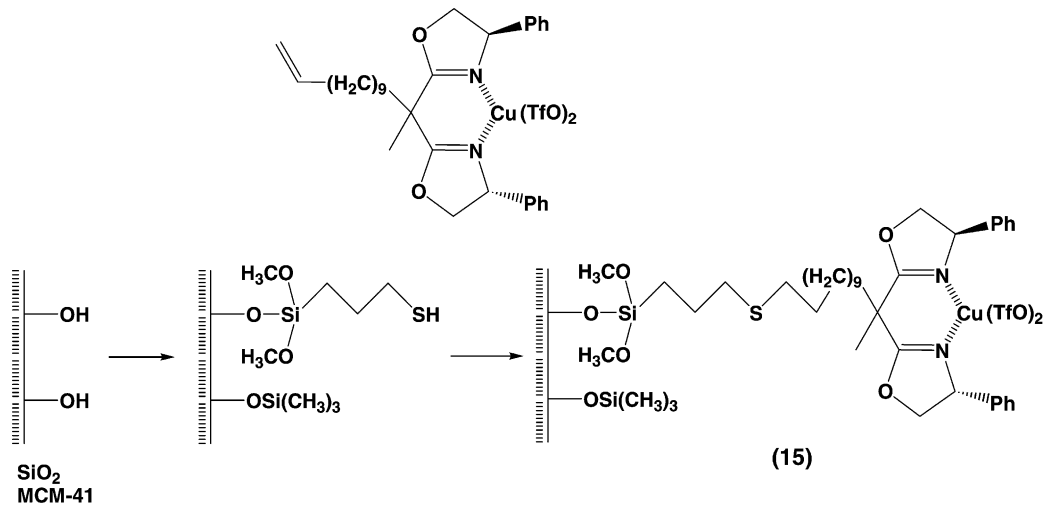

Fig. 9. Schematic procedure of the immobilized Cu-oxazoline catalysts for the Friedel–Crafts hydroxyalkylation. The Cu complex was attached on SiO_2 surface via an anchored oxazoline ligand.

recycled with the similar conversion and high enantioselectivity.

In homogeneous phases, asymmetric syntheses on metal complexes have been successfully accomplished, but heterogenization of asymmetric catalysts has been still difficult. Oxide-supported chiral metal complexes that are favorable for separation, recycling, handling, etc. may be a promising catalytic system composed of new catalytic materials beyond the present homogeneous asymmetric catalysts.

8. Molecular imprinting

Native enzyme catalysts can recognize particular substrate molecules at active centers which possess reaction spaces with spatially organized molecular recognition sites. To prepare artificial enzymatic systems possessing molecular recognition ability for particular molecules, molecular imprinting methods which create template-shape cavities with memory of the template molecules in polymer matrices have been developed [40–46] and established in receptor, chromatographical separations, fine chemical sensing, etc. in the past decade. Molecular design of catalytic sites is necessary for regulation of catalysis. The regulation of dynamic catalytic processes requires careful strategy for chemical design of the catalytic sites. Recently, in addition to imprinted acid–base catalysts, some examples of molecular imprinting of metal complexes have been reported and constitute state of the arts currently.

8.1. Application of molecular imprinting to metal complexes

Principle of creation of cavity with similar shape to template molecule in appropriate matrix by molecular imprinting involves two processes illustrated in Fig. 10. Organic or inorganic polymer matrix is produced around a particular molecule used as a template, covering the space around the template. Then the template molecule is removed from the polymer matrix, and as the result, template-shape cavity behind the template is obtained in the matrix. The cavity acts as selective recognition space for molecules with similar shape to the template.

In the last half of the century, various materials were prepared by simple imprinting processes mimicking shapes of template molecules. These materials were applied to separation and sensing processes which are regulated by simple adsorption on the imprinted sites. However, regulation of catalytic reactions has been still hard because catalysis is a dynamic process involving rearrangement of chemical bonds in the substrate molecules. Nevertheless, artificial enzymatic materials synthesized by molecular imprinting techniques using a variety of template molecules provide promising molecular recognition catalysis with 100% selectivity for a variety of catalytic reactions where natural enzymes can not be employed.

Recently, in addition to imprinted acid-base catalysts [47–53], attempts to imprint metal complexes have been reported. The catalytic applications are summarized in Table 7. In most cases of metal-complex

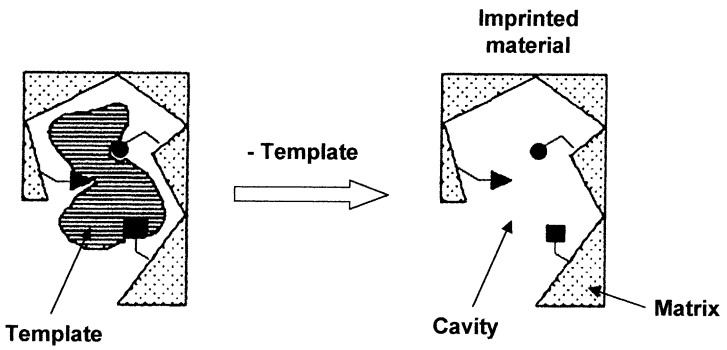

Fig. 10. Principle of molecular imprinting to prepare template-shape cavity. Template-shape space leaves in polymer matrix behind the template molecule.

Table 7
Reported molecular-imprinting metal-complex catalysts

Metal	Catalytic reaction	Description	Reference
Co	Aldol condensation	Bulk imprinting of diketone mimicking a reaction intermediate	[53]
Rh	Hydride transfer reduction of ketones	Bulk polymer imprinting of a reaction intermediate	[54]
Ti	Diels–Alder reaction	Ti complex linked by polymerizable ligands in styrene polymer	[55]
Ru	Transfer hydrogenation of ketones	Bulk imprinting of phosphinate analog of an intermediate	[56]
Rh	Transfer hydrogenation of ketones	Bulk imprinting of phosphinate analog of an intermediate	[57]
Pd	Cross coupling reaction	Attaching in styrene-divinylbenzene copolymer matrix	[58]
Rh	Hydrogenation of alkenes	Surface imprinting of $P(OCH_3)_3$ ligand of attached Rh monomer	[59]
Rh	Hydrogenation of alkenes	Surface imprinting of $P(OCH_3)_3$ ligand of attached Rh dimer	[60,61]

imprinting, ligands of the complexes are used as template molecules, which aims to create cavity near the metal site. Molecular imprinting of metal complexes enables to realize several features to note, (1) attachment of metal complex on robust supports, (2) surrounding of the metal complex by polymer matrix, (3) formation of new active structure in the matrix, and (4) production of shape selective space on the metal site. Metal complexes thus imprinted have been applied to molecular recognition [54,55], reactive complex stabilization [56,57], ligand exchange reaction [58], and catalysis [59–67].

Most of the imprinted metal-complex catalysts have been prepared by imprinting in bulk polymer. However, active sites prepared by bulk imprinting may often be located inside the bulk polymer matrices, where access of substrate molecules to the sites is difficult. Further, such organic polymers tend to be undurable in organic solvents or under severe catalytic conditions such as in the presence of oxidants, at high temperatures, etc. On the other hand, oxide supports are inert and robust materials, on which metal complexes can be attached by chemical bondings. As described above, oxide-supported metal complexes often exhibit unique property and remarkable reactivity so that molecular imprinting of metal complexes at oxide surfaces has many possibilities to produce new excellent catalysts similar to enzymatic systems. However, molecular imprinting of metal complexes at oxide surfaces had been not reported before our study. Very recently, we have succeeded in preparing imprinted rhodium complexes at Ox.50 (SiO_2) surface for catalytic shape-selective hydrogenation of simple alkenes without any functional group [65–67]. Recognition of simple alkenes without any functional group is generally difficult. Here, we introduce our recent works of molecular imprinting metal-complex catalysts, which show remarkable catalytic performances beyond simply supported metal-complex catalysts. These are the first attempts to imprint metal complexes on oxide surfaces and to investigate their catalytic properties.

8.2. Molecular imprinting of Rh monomers at SiO_2 surface

Imprinting at surfaces can provide catalytic sites readily accessible for reactant molecules and more uniform locations of imprinted sites compared to bulk imprinting. Our approach of surface molecular imprinting for preparation of metal complex catalysts is accomplished by combining two techniques, (1) attachment of metal-complex on oxide surface and (2) molecular imprinting for ligand of the attached metal complex at the surface. Since a template with the same shape as the transition state of a rate-determining step is most appropriate for catalyst design, but it is hard to estimate its accurate structure. Reaction intermediates before and after the rate-determining step may be considered to have similar shapes to the early and late transition states, respectively, and they are generally used as templates for molecular imprinting catalysts. Our strategy is to use a ligand as template. Ligands of a metal complex not only influence its catalytic activity but also provide an unsaturated, reactive metal site with a ligand-shape space by removal of a ligand. We chose a ligand of the attached metal complex with the similar shape to a reaction intermediate of alkene hydrogenation as a template molecule. $P(OCH_3)_3$ ligand has a similar shape to one of the half-hydrogenated species of 3-ethyl-2-pentene, which can produce the intermediate-shape cavity by extraction of the ligand.

Our strategy to design active and selective catalysts was based on the following five factors for regulation: (1) conformation of ligands coordinated to Rh atom, (2) orientation of vacant site on Rh, (3) cavity with the template molecular shape for reaction space produced behind template removal, (4) architecture of the cavity wall, and (5) micropore in inorganic polymer-matrix overlayers stabilizing the active species at the surface.

Attaching and molecular imprinting of Rh monomers were performed by following procedure as shown in Fig. 11 [65]. First, we prepared a new SiO_2-attached Rh-monomer catalyst (Rh_{sup} catalyst), which has two $P(OCH_3)_3$ ligands per Rh by supporting $RhCl(P(OCH_3)_3)_3$ precursor on SiO_2 (Ox.50) and subsequent evacuation at 363 K. Second, we performed the hydrolysis-polymerization of $Si(OCH_3)_4$ on the attached Rh monomers on Ox.50 surface to create a novel imprinted Rh_{imp} catalyst with template-shape cavity by removal of one of the two $P(OCH_3)_3$ ligands (Rh_{imp} catalyst). $P(OCH_3)_3$ can be regarded to be an analogue of a half-hydrogenated alkyl intermediate in hydrogenation of 3-ethyl-2-pentene.

Stacking of SiO_2-matrix overlayers produced at the Ox.50 surface by deposition of $Si(OCH_3)_4$ and subsequent hydrolysis-polymerization was characterized by ^{29}Si solid-state MAS NMR and XPS. After the polymerization, new ^{29}Si NMR signals attributed to the piled SiO_2 overlayers appear in Fig. 12(a1). Accompanied with increasing stacking of SiO_2-matrix overlayers, XPS Rh 3d peak intensities reduce, which indicates that space around the attached Rh complex is covered by the SiO_2 matrix. Note that the SiO_2 network does not cover top of the attached Rh complex, but makes micropores including the attached Rh complex on the surface as shown in Fig. 11. Existence of micropores in the SiO_2-matrix overlayers is confirmed by *t*-plots in Fig. 12(b). There is no break in *t*-plot for the SiO_2-matrix overlayers without Rh complexes, where there is no uniform micropores. The supported Rh_{sup} catalyst without SiO_2-matrix overlayers and the $Rh_{imp\text{-}1.4}$ sample with 1.4 ML (0.57 nm thick) SiO_2-matrix overlayers (Fig. 12(b1)) are both regarded to be nonporous materials. Fig. 12(b2), (b3) and (b4) represent *t*-plots for the $Rh_{imp\text{-}4.7}$, $Rh_{imp\text{-}9.3}$, and $Rh_{imp\text{-}15.9}$ catalysts with the SiO_2-matrix overlayers of 4.7 ML (1.9 nm), 9.3 ML (3.8 nm), and 15.9 ML (6.4 nm), respectively, which demonstrate formation of micropores by the imprinting. The micropore diameters were estimated to be 0.67, 0.64, and 0.60 nm, for the $Rh_{imp\text{-}4.7}$, $Rh_{imp\text{-}9.3}$, and $Rh_{imp\text{-}15.9}$ catalysts, respectively.

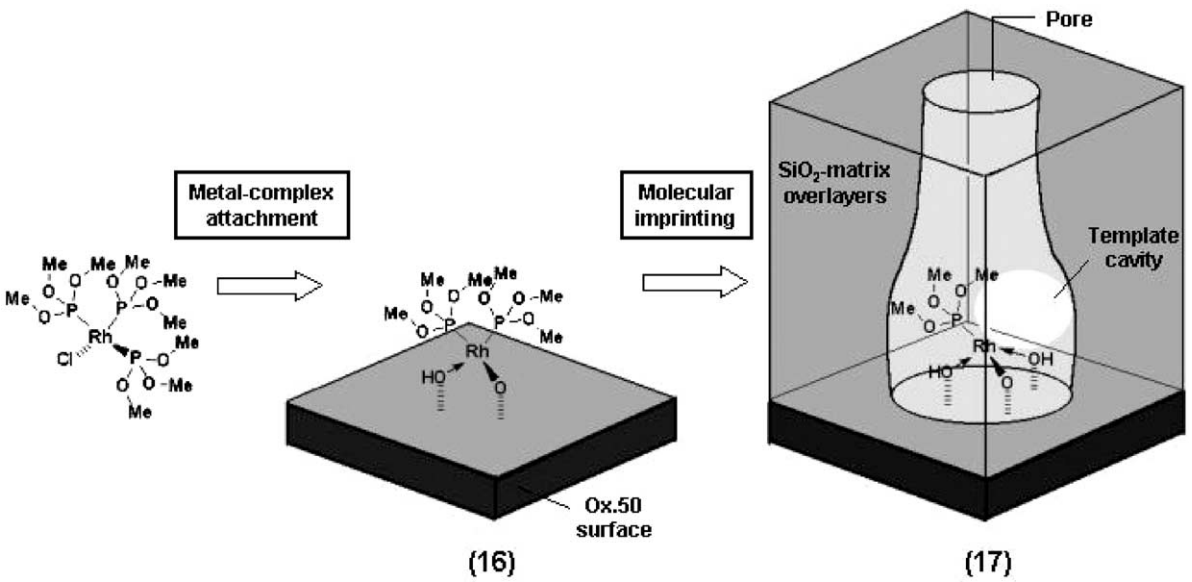

Fig. 11. Preparation steps for the imprinted Rh-monomer catalyst on SiO_2 surface. A $P(OCH_3)_3$ ligand coordinated with the attached Rh complex corresponds to the template for a half-hydrogenated species of 3-ethyl-2-pentene.

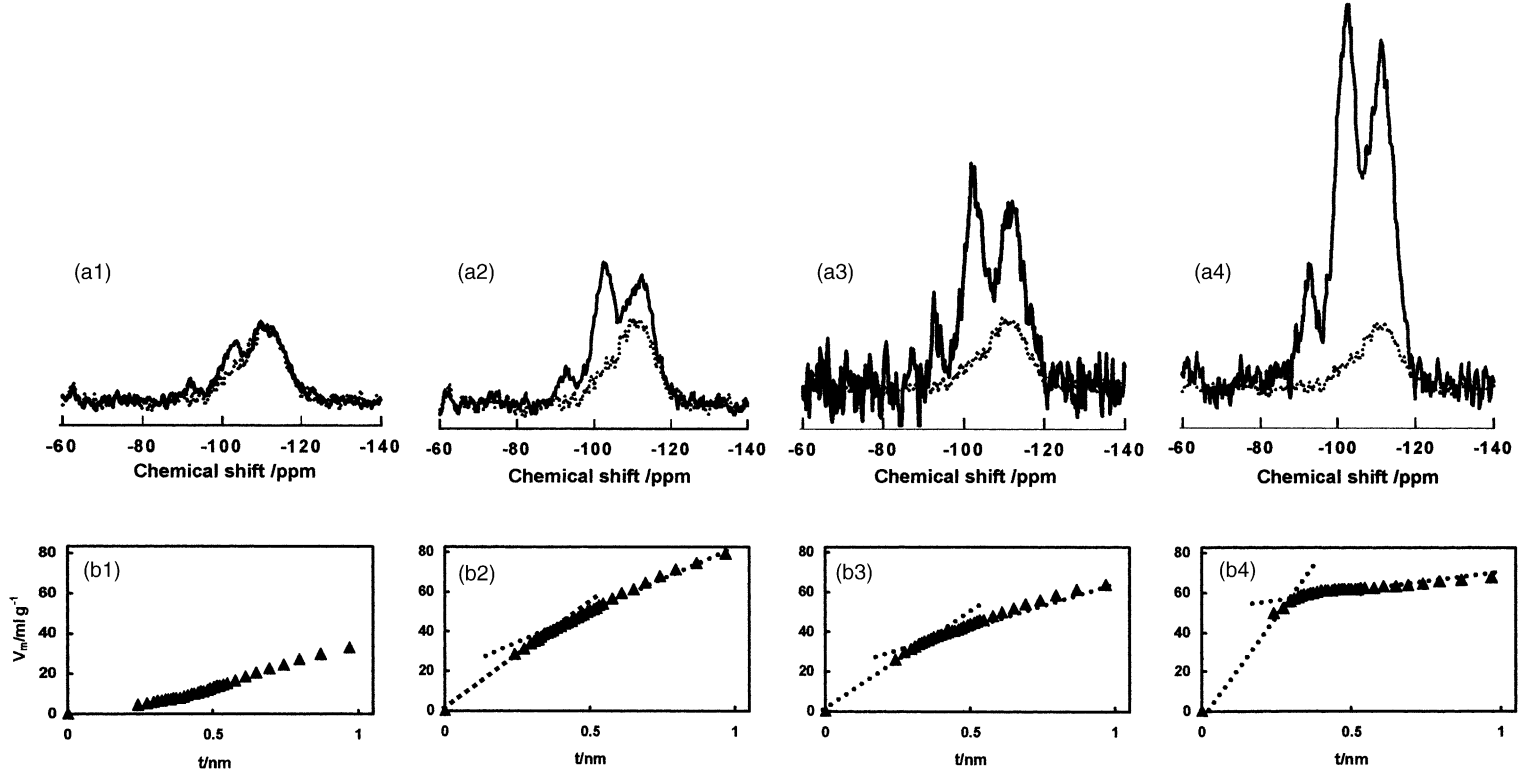

Fig. 12. (a) ^{29}Si solid-state MAS NMR spectra for the imprinted Rh-monomer catalysts and (b) their *t*-plots of N_2 adsorption. (1) 1.4 ML SiO_2-matrix overlayer, (2) 4.7 ML SiO_2-matrix overlayer (pore diameter: 0.67 nm), (3) 9.3 ML SiO_2-matrix overlayer (pore diameter: 0.64 nm), and (4) 15.9 ML SiO_2-matrix overlayers (pore diameter: 0.60 nm).

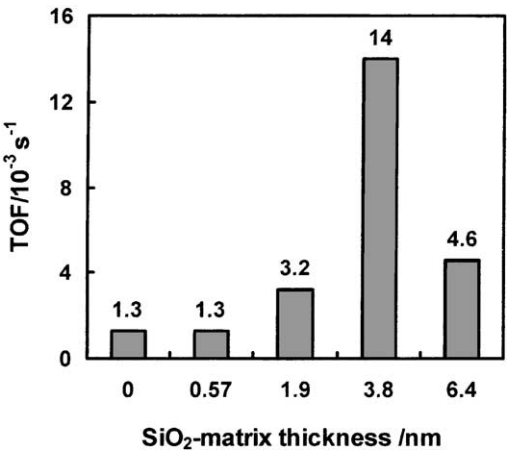

Fig. 13. Catalytic activities for 2-pentene hydrogenation at 348 K on the supported (Rh_{sup}) and imprinted (Rh_{imp}) Rh-monomer catalysts with different stacking of the SiO_2-matrix overlayers.

The catalytic activity of the Rh complex for hydrogenation of 2-pentene remarkably depends on the height of the SiO_2-matrix overlayers as shown in Fig. 13. Attended to an increase of the height of the SiO_2-matrix overlayers, the 2-pentene hydrogenation activity swells widely and reaches the activity 11 times higher compared to that of the supported catalyst (Rh_{sup}) after stacking of SiO_2-matrix overlayers of 3.8 nm thick. As 2-pentene is small enough compared to the template, such a significant increase of the catalytic activity shows a change of the structure of active Rh sites to more reactive one. Further increase in the amount of SiO_2-matrix overlayers reduces the catalytic activity to 33% of the maximum activity. The increase of the hydrogenation activity by the imprinting is due to a change in the surface-attached rhodium structure as characterized by Rh K-edge EXAFS analysis [65]. The Rh monomers with the SiO_2-matrix overlayers of 3.8 and 6.4 nm thick were characterized to have one $P(OCH_3)_3$ on Rh in a tridentate form as illustrated in Fig. 11, which indicates removal of a template ligand $P(OCH_3)_3$ per Rh in the imprinting step. The removal of one of the two $P(OCH_3)_3$ ligands by the surface imprinting provides the cavity of the template shape for the catalytic reaction as illustrated in Fig. 11. The increase of hydrogenation activities is ascribed to formation of the coordinatively unsaturated structure. It seems form the EXAFS analysis that the removal of a template ligand is incomplete for the samples of 0.57 and 1.9 nm thick [65]. Thus, the imprinting provides the active Rh_{imp} monomer structure with the template cavity. It is to be noted that the active $Rh_{imp\text{-}9.3}$ catalyst is air-stable and highly durable for the catalytic hydrogenation due to the location and chemical attachment of the Rh monomers at the bottom in the micropores of the SiO_2-matrix overlayers on the Ox.50 surface. The decrease in the activity of the $Rh_{imp\text{-}15.9}$ catalyst with 15.9 ML SiO_2 overlayers may be due to a pile of the micropores and/or partial decomposition of the unsaturated active Rh structures, by the addition hydrolysis-polymerization of $Si(OCH_3)_4$.

The large ligand $P(OCH_3)_3$ in the Rh monomer can regulate the reactivity of the metal center electronically and geometrically to give higher selectivity than metal and metal oxide catalysts without any ligand. The selectivity of the surface-attached Rh monomers is also subjected to regulation by the surface which is regarded as a unique and large ligand. The supported Ru_{sup} catalyst showed high selectivity for the alkene hydrogenation as shown in Fig. 14. Hydrogenation of linear alkenes like 2-pentene, -hexene, -heptene, and -octene without any branch alkyl group are very fast, while branch alkenes such as 3-methyl-2-pentene, 4-methyl-2-pentene, 3-ethyl-2-pentene, etc. are hard to hydrogenate compared with the linear alkenes. Length of the alkene main chain does not affect the reaction rates.

Selectivity for the alkene hydrogenation on the imprinted Rh_{imp} catalyst depended on the size and shape of the template cavity in the micropores of the SiO_2-matrix overlayers on the Ox.50 surface in addition to the electronic and geometric effects of the ligands of the Rh complex. To examine the molecular imprinting effect on the selectivity, the ratios of TOFs of the imprinted catalyst to TOFs of the supported catalyst for each alkene are compared in Table 8. The difference in the TOF ratios between 3-methyl-2-pentene and 3-ethyl-2-pentene is so large, where the difference in the length of the branch group between methyl and ethyl is discriminated on the imprinted catalyst. The difference in the branch groups between methyl and ethyl is also observed for the hydrogenation of 4-methyl-2-pentene and 4-methyl-2-hexene. The TOF ratio for 4-methyl-2-hexene is much smaller than that for 2-pentene, where the alkenes are different with each other in the size and shape of the

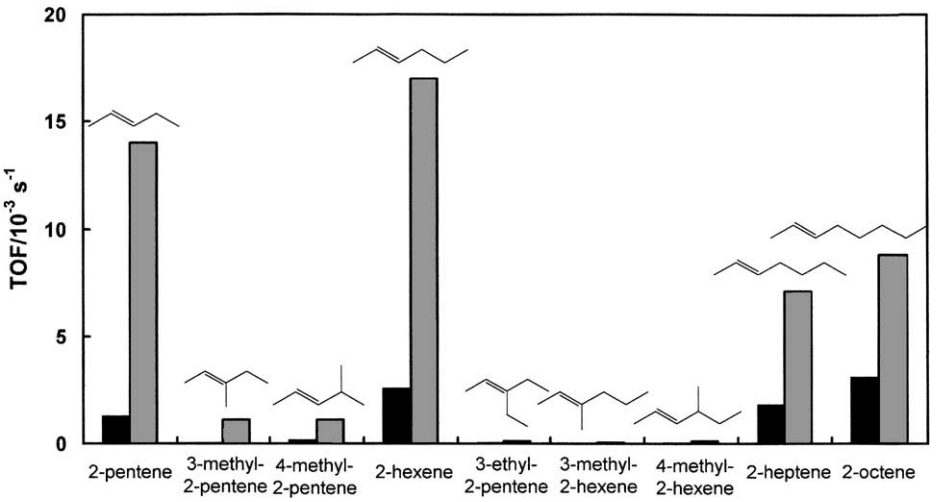

Fig. 14. Turnover frequencies (TOFs) of the alkene hydrogenation on the supported (Rh_{sup}) (black) and imprinted (Rh_{imp}) (gray) Rh-monomer catalysts.

ethyl group. There is also a big difference between 2-pentene and -heptene, where an ethyl group of the alkene main chain is discriminated. Thus, the molecular imprinting catalyst can discriminate the size and shape of the alkenes without functional groups. It is noteworthy that the reaction rates of the linear alkenes such as 2-pentene, -hexene, -heptene, and -octene on the supported Rh_{sup} catalyst are similar to each other, whereas on the imprinted Rh_{imp} catalyst the rate enhancements (TOF ratios) for 2-hepente and -octene (3.9 and 2.8 times, respectively) are much less than those for 2-pentene and -hexene (11 and 6.5 times, respectively). Because the length of linear alkene chains can not be discerned by the ligand-coordinated metal site in the supported Rh_{sup} catalyst, it is concluded that the difference is caused by the space and shape

Table 8
Degrees of the enhancement of the reaction rates by molecular imprinting (ratios of TOFs), activation energies (E_a), activation enthalpies ($\Delta^{\ddagger}H$), and activation entropies ($\Delta^{\ddagger}S$) for the catalytic hydrogenation of alkenes on the Rh-monomer catalysts[a]

	Reactant	Ratio of TOFs[b]	Supported catalyst			Imprinted catalyst		
			E_a[c]	$\Delta^{\ddagger}H$[d]	$\Delta^{\ddagger}S$[e]	E_a[c]	$\Delta^{\ddagger}H$[d]	$\Delta^{\ddagger}S$[e]
C_5	2-Pentene	11	35	32	−202	33	30	−188
C_6	3-Methyl-2-pentene	13	42	39	−205	38	35	−195
	4-Methyl-2-pentene	6.9	38	35	−211	41	38	−186
	2-Hexene	6.5	29	26	−213	27	24	−203
C_7	3-Ethyl-2-pentene	3.4	43	40	−209	11	8	−291
	3-Methyl-2-hexene	–		Negligible TOF		13	10	−295
	4-Methyl-2-hexene	2.4	43	40	−206	9	6	−296
	2-Heptene	3.9	31	28	−211	11	8	−257
C_8	2-Octene	2.8	29	26	−212	10	7	−259

[a] Rh/alkene/toluene = 1/1000/23000, H_2 = 101.3 kPa.
[b] TOF of the $Rh_{imp\text{-}9.3}$ catalyst/TOF of the Rh_{sup} catalyst, at 348 K.
[c] E_a: kJ mol^{-1}.
[d] $\Delta^{\ddagger}H$: kJ mol^{-1}.
[e] $\Delta^{\ddagger}S$: J K^{-1} mol^{-1}.

of the template cavity at the imprinted Rh monomer site.

It is well known that the alkene hydrogenation mechanism involves four steps; (1) dissociation of hydrogen on metal center to form hydrides, (2) coordination of alkene C=C double bond to the metal center, (3) insertion to the Rh–H bond to form a half-hydrogenated alkyl species, and (4) reaction of the alkyl with remaining hydride to form alkane. The rate-determining step has been experimentally and theoretically considered to be the third step (alkyl formation). The activation energies for the alkene hydrogenation on the supported Rh_{sup} catalyst in Table 8 are ca. 30 kJ mol^{-1} and ca. 40 kJ mol^{-1} for linear alkenes and branch alkenes, respectively, which are typical values for the activation energies on metal-complex catalysts. The activation entropies for the catalytic hydrogenation on the Rh_{sup} catalyst are similar values for all the alkenes used in Table 8. The activation energies and activation entropies for the hydrogenation of the C_5 and C_6 alkenes do not change significantly after the imprinting (Table 8). These results demonstrate that the rate-determining step for the hydrogenation of C_5 and C_6 alkenes on the supported and imprinted catalysts is the same as that for the Wilkinson complex catalyst and the catalytic hydrogenation of the smaller alkenes than the template is not regulated by the template cavity.

In contrast, the activation energies for the larger C_7 and C_8 alkenes with different shapes from the template $P(OCH_3)_3$ on the imprinted Rh_{imp} catalyst are so small as 9–13 kJ mol^{-1} (Table 8). These dramatic decrease in the activation energy together with the small TOF ratios (less promotion) discussed above, indicates shift of the rate-determining step from the alkyl formation to π-coordination of alkene to Rh. Associated with this shift, the activation entropies for the hydrogenation of those alkenes on the Rh_{imp} catalyst also decrease largely to −257 to −295 from −206 to −212 J mol^{-1} K^{-1} for the Rh_{sup} catalyst. The values of −257 to −295 J mol^{-1} K^{-1} are also much smaller than the values of −186 to −203 J mol^{-1} K^{-1} for the smaller alkenes. The decrease in the activation entropy suggests that conformation of the coordinated alkene in the template cavity is strongly regulated by shape of the template cavity and the remaining $P(OCH_3)_3$ ligand. The C_7 and C_8 alkenes stick out of the template cavity in the Rh_{imp} catalyst. It is to be noted that the shape of alkenes without any functional group can be significantly discriminated on the imprinted catalyst.

8.3. Molecular imprinting of Rh dimers at SiO_2 surface

We have also prepared a new Rh-dimer molecular imprinting catalyst (Rh_{2imp}) at a SiO_2 surface for hydrogenation of alkenes. The preparation steps are presented in Fig. 15 [66,67]. In heterogeneous systems, generally metal–metal interaction is crucial to dissociate hydrogen molecules, which is most relevant to hydrogenation. The metal dimer is regarded as a minimum active structure for heterogeneous metal catalysis involving metal–metal bonding. In order to create a Rh dimer structure with a template cavity on Ox.50 surface, a $Rh_2Cl_2(CO)_4$ and $P(OCH_3)_3$ were used as a Rh dimer precursor and a template ligand, respectively. The template $P(OCH_3)_3$ is regarded as an analogue to a half-hydrogenated alkyl intermediate of hydrogenation of 3-ethyl-2-pentene.

$Rh_2Cl_2(CO)_4$ is attached on the Ox.50 surface retaining its dimer structure monitored by FT-IR [66]. By exposing to $P(OCH_3)_3$, the surface-attached Rh carbonyl dimer is converted to Rh monomer pair (Rh_{2sup}) with two $P(OCH_3)_3$ ligands on Rh (Rh–P: 0.224 nm), which is attached on the surface via Rh–O bonding at 0.203 nm in a bidentate form. The first step of molecular imprinting for the attached rhodium complexes is performed by hydrolysis–polymerization of $Si(OCH_3)_4$, which possesses methoxy groups with positive interaction with the template. The second step is removal of a template by evacuation at 363 K. By the imprinting procedure, Rh 3d XPS intensity reduces remarkably [66]. Note that the surface imprinting causes dimerization of the Rh monomers to produce highly active Rh dimers with a direct Rh–Rh bond at 0.268 nm in the pores of 0.74 nm dimension in the SiO_2-matrix overlayers. The EXAFS Fourier-transforms are shown in Fig. 16. The EXAFS analysis also characterizes the removal of a phosphite ligand per Rh by the molecular imprinting procedure, where the coordination number of Rh-P bond at 0.221 nm reduces from 2.3 to 1.1.

The change in Rh structures in the imprinting processes can be explained by DFT calculation [66]. Five structural models on a silica cluster substrate, $[Rh(P(OCH_3)_3)_2]_2$, $Rh(P(OCH_3)_3)$–$Rh(P(OCH_3)_3)_2$,

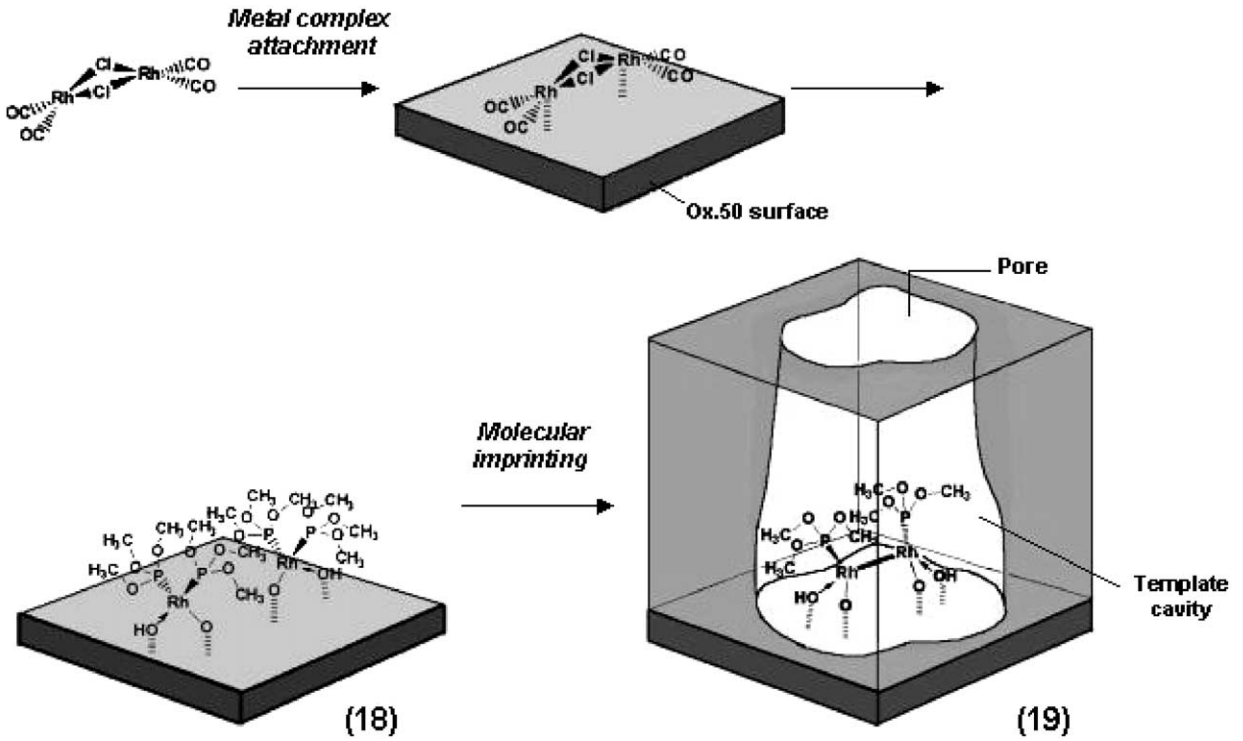

Fig. 15. Scheme for attaching of the imprinted Rh dimer (Rh_{2imp}) on Ox.50 surface and following molecular imprinting on the surface.

$Rh_2(P(OCH_3)_3)_3$, P-bridged $Rh_2(P(OCH_3)_3)_3$, and $Rh_2(P(OCH_3)_3)_2$, were calculated, which are regarded as models for the Rh-monomer pair catalyst (Rh_{2sup}), possible intermediate species with three $P(OCH_3)_3$ ligands, and the imprinting Rh-dimer catalyst (Rh_{2imp}), respectively. The optimized structures and energy profiles for those model species are illustrated in Fig. 17 [66]. Initial structures of each Rh

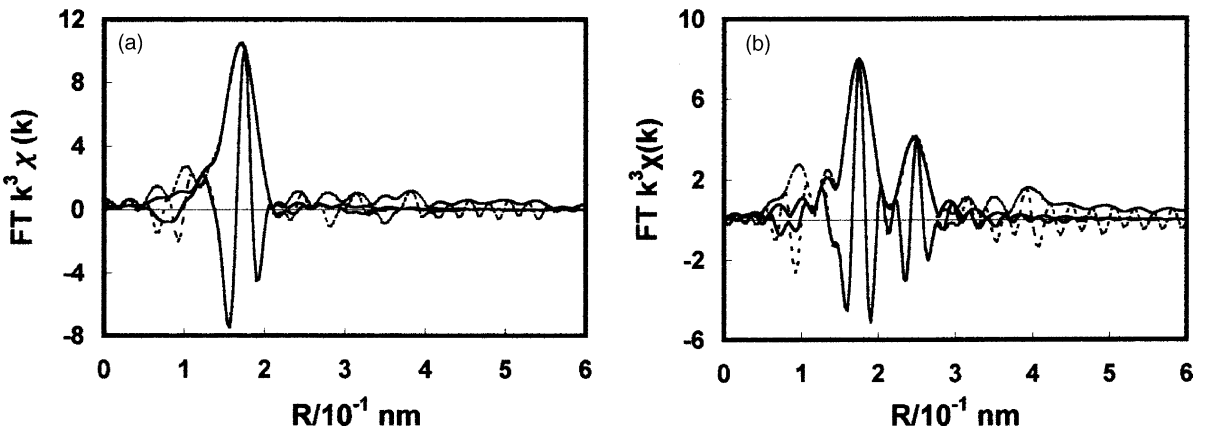

Fig. 16. k^3-weighted Fourier-transforms for the Rh K-edge EXAFS spectra measured at 15 K and their curve-fitting results for the supported (Rh_{2sup}) (a) and imprinted (Rh_{2imp}) (b) Rh-dimer catalysts.

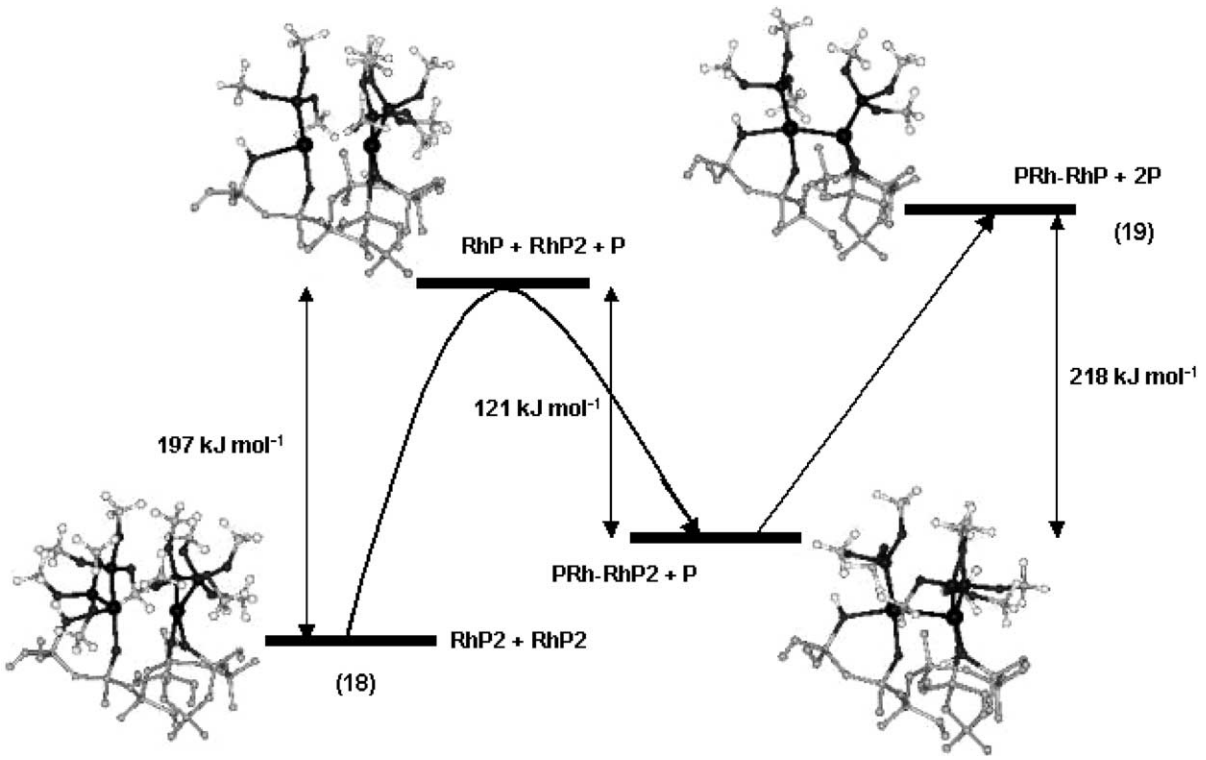

Fig. 17. Energy profiles in the imprinting steps for the Rh-dimer catalyst by DFT calculation.

complex including the SiO_2 substrate was obtained by the Molecular Mechanics (MM) method with the Universal force field 1.02. $[Rh(P(OCH_3)_3)_2]_2$ with four $P(OCH_3)_3$ ligands per two Rh atoms is the most stable complex with a Rh–Rh distance of 0.306 nm, which is indicative of no direct bonding between Rh atoms. $Rh_2(P(OCH_3)_3)_3$ with three $P(OCH_3)_3$ ligands per two Rh atoms is the second most stable complex with a Rh–Rh distance of 0.271 nm. This result implies that the removal of one phosphite ligand is compensated by the formation of Rh–Rh bond. In order to gain insight into this process, one of four $P(OCH_3)_3$ ligands in $[Rh(P(OCH_3)_3)_2]_2$ was removed, while the Rh–Rh bond was fixed at 0.306 nm. An optimized structure for $Rh_2(P(OCH_3)_3)_3$ is depicted in Fig. 17, which becomes unstable. The energy difference (197 kJ mol^{-1}) roughly estimated indicates the presence of activation energy for the ligand removal, but the real transition state may involve Rh–Rh bonding at the shorter distance than 0.306 nm, resulting in a decrease in the activation energy. It is to be noted that during the transformation of the supported Rh catalyst to the imprinted Rh catalyst there is a stable structure of $Rh_2(P(OCH_3)_3)_3$ with one phosphite ligand on a Rh atom and with two phosphite ligands on another Rh atom. A bridge bonded structure with a bridge $P(OCH_3)_3$, which might be possible for $Rh_2(P(OCH_3)_3)_3$, is unstable by 59 kJ mol^{-1} compared to the non-bridged $Rh_2(P(OCH_3)_3)_3$ according to the DFT calculation. Further loss of one of the two $P(OCH_3)_3$ ligands on a Rh atom leads to the formation of $Rh_2(P(OCH_3)_3)_2$ (Rh_{2imp} catalyst) with expense of the energy (Fig. 17).

We assume that the elimination of the two phosphite ligands from the monomer pair to produce the $Rh_2(P(OCH_3)_3)_2$ structure (Rh_{2imp} catalyst) occurs step by step via the stable intermediate $Rh_2(P(OCH_3)_3)_3$ with one $P(OCH_3)_3$ on a Rh atom and with two $P(OCH_3)_3$ on another Rh atom in the dimer at the Rh–Rh bond of 0.271 nm. Therefore, the stable intermediate $Rh_2(P(OCH_3)_3)_3$ is the imprinted Rh species under the CVD process at 348 K. The

Table 9
Steady-state catalytic activities (TOF (s^{-1})) of the Rh catalysts for hydrogenation of eight alkenes under 101.3 kPa of H_2 in toluene solution[a]

Reactant	$Rh_2Cl_2(CO)_4$[b]	$RhCl(P(OCH_3)_3)_3$[b]	$Rh_2Cl_2(CO)_4/SiO_2$	Rh_{2sup} catalyst	Rh_{2imp} catalyst
2-Pentene	–	–	–	1.3×10^{-3}	6.6×10^{-2}
3-Methyl-2-pentene	–	–	–	7.0×10^{-5}	3.6×10^{-3}
4-Methyl-2-pentene	–	–	–	1.3×10^{-4}	5.9×10^{-3}
3-Ethyl-2-pentene	0[c]	0	0[c]	4.4×10^{-5}	1.5×10^{-3}
2,4,4-Trimethyl-2-pentene	–	–	–	0	1.3×10^{-4}
4-Methyl-2-hexene	0[c]	0	0[c]	6.8×10^{-5}	9.6×10^{-4}
2-Octene	0[c]	0	0[c]	3.0×10^{-3}	3.0×10^{-2}
1-Phenylpropene	–	–	–	2.8×10^{-3}	2.0×10^{-2}

[a] Rh/alkene/toluene = 1/1000/23000 (molar ratio).
[b] Homogeneous system.
[c] Decomposition of Rh complex was observed.

elimination of a template $P(OCH_3)_3$ ligand from the intermediate at 363 K under vacuum generates the template size cavity in the SiO_2-matrix overlayers.

Table 9 shows steady-state reaction rates (turnover frequencies (TOF)) of the hydrogenation of eight alkenes at 348 K on the supported Rh-complex catalyst (Rh_{2sup}) and the molecular imprinting catalyst (Rh_{2imp}). The homogeneous complexes $Rh_2Cl_2(CO)_4$ and $RhCl(P(OCH_3)_3)_3$ and the supported species $Rh_2Cl_2(CO)_4/SiO_2$ show no activities for the reaction. On the other hand, the Rh_{2sup} catalyst exhibits significant catalytic activities under the similar reaction conditions. It is to be noted that the hydrogenation reactions are remarkably promoted for all alkenes by the surface imprinting. The imprinted Rh_{2imp} catalyst is tremendously active for the alkene hydrogenation. For example, hydrogenation of 2-pentene is promoted 51 times as compared to that on the supported Rh catalyst. The metal–metal bonding and coordinative unsaturation of the Rh dimer are key factors for the remarkable activity of the Rh_{2imp} catalyst. The Rh_{2imp} catalyst is highly durable and surprisingly air-stable in spite of its unsaturated structure, which is advantageous in practical handling of the system. Further, it can be reused without any loss of the catalytic activity.

H_2 adsorption on the Rh_{2imp} catalyst is irreversible and its amount at saturation was estimated to be 0.92 H_2/Rh dimer. Thus, most of the Rh sites in the Rh_{2imp} catalyst are converted to have monohydride species under the hydrogenation conditions.

Structures around Rh atoms in the Rh_{2imp} catalyst at each step of the alkene hydrogenation were investigated by EXAFS at 15 K (Table 10) [67]. The Rh dimer after H_2 adsorption exhibits similar EXAFS oscillation and Fourier-transform to those for the fresh imprinted catalyst. The detailed analysis of the EXAFS data confirmed retention of the local conformation of the Rh dimer with a Rh–Rh bond (coordination number (CN): 1.3 ± 0.4), two Rh–O bonds (CN: 1.7 ± 0.5), and a Rh–P bond (CN: 1.2 ± 0.2). But contraction of Rh–Rh bond from 0.268 nm ($\pm$ 0.001 nm) to 0.265 nm ($\pm$0.001 nm) was found with the hydride dimer, which indicates stabilization of the dimer structure by electronic rearrangement due to hydride coordination on both Rh atoms in the dimer

Table 10
Structural parameters of EXAFS curve-fitting analyses for the imprinted Rh-dimer catalysts (Rh_{2imp})[a]

Shell	CN	R ($\times 10^{-1}$ nm)	s^2 ($\times 10^{-2}$ nm^2)
Fresh[b]			
Rh–O	2.0 ± 0.5	2.11 ± 0.02	$(4 \pm 3) \times 10^{-3}$
Rh–P	1.1 ± 0.2	2.21 ± 0.01	$(1 \pm 2) \times 10^{-3}$
Rh–Rh	1.3 ± 0.3	2.68 ± 0.01	$(7 \pm 1) \times 10^{-3}$
After H_2 adsorption[c]			
Rh–O	1.7 ± 0.5	2.08 ± 0.03	$(6 \pm 3) \times 10^{-3}$
Rh–P	1.2 ± 0.2	2.20 ± 0.01	$(2 \pm 4) \times 10^{-3}$
Rh–Rh	1.3 ± 0.4	2.65 ± 0.01	$(7 \pm 2) \times 10^{-3}$
After reaction of the H_2-adsorbed sample with 3-methyl-2-pentene[d]			
Rh–O	2.2 ± 0.6	2.12 ± 0.03	$(5 \pm 4) \times 10^{-3}$
Rh–P	1.1 ± 0.2	2.21 ± 0.01	$(1 \pm 4) \times 10^{-3}$
Rh–Rh	1.2 ± 0.4	2.70 ± 0.01	$(6 \pm 2) \times 10^{-3}$

[a] Measured at 15 K.
[b] $\Delta E_0 = 11 \pm 2$ eV, $R_f = 0.3\%$.
[c] $\Delta E_0 = 9 \pm 4$ eV, $R_f = 1.6\%$.
[d] $\Delta E_0 = 12 \pm 3$ eV, $R_f = 1.4\%$.

(Table 10). After reaction of the Rh-dimer hydride species with 3-methyl-2-pentene, the shrunk Rh–Rh bond of the monohydride species expanded again to recover the initial bond length. During the hydrogenation process, the Rh–Rh bond is retained without any breaking of the bond. Further, the bond distances and coordination numbers for Rh–O and Rh–P did not change significantly (Table 10). The EXAFS analysis demonstrates that the alkene hydrogenation on the molecular imprinting Rh_{2imp} catalyst proceeds on the Rh dimer unit in each step of the catalytic cycle. It seems that the chemical attachment in a tetradentate form (Rh–O: 0.211 nm) and the location with stable fitting in the micropore of 1.9 nm thick prevent the Rh dimers from leaching to the reaction solution and decomposing and gathering of the Rh dimers.

Ratios of TOFs corresponding to degree of enhancement of the reaction rates by the imprinting revealed that the imprinted Rh-dimer catalyst (Rh_{2imp}) showed size and shape selectivities for the alkenes as shown in Fig. 18. Selectivity for the alkene hydrogenation on the Rh_{2imp} catalyst depends on the size and shape of the template cavity as reaction site in the micropores of the SiO_2-matrix overlayers on the Ox.50 surface in addition to the electronic and geometric effects of the ligands. The TOF ratios reduce with gain of alkene size as shown in Fig. 18. It is to be noted that there is a large decrease between 3-ethyl-2-pentene and 4-methyl-2-hexene (4-ethyl-2-pentene) due to the difference in the shape of the alkenes. The difference in the TOF ratios between 4-methyl-2-pentene and 4-methyl-2-hexene is also large, where the difference in the size of a methyl group is discriminated on the Rh_{2imp} catalyst. The TOF ratio for 4-methyl-2-hexene is much smaller than that for 2-pentene, where the difference is referred to the ethyl group. There is also a big difference between 2-pentene and -octene, where a propyl group can be discriminated. Thus, the molecular imprinting catalyst discriminates the size and shape of the alkenes. However, there was no significant difference in the TOF ratios between 2-pentene and 4-methyl-2-pentene, between 3-methyl-2-pentene and 3-ethyl-2-pentene, and between 2-pentene and 3-ethyl-2-pentene (Fig. 18). Thus, the molecular imprinting catalyst can not discriminate the existence of methyl and ethyl groups among the smaller alkenes than the template size. It is noteworthy that the reaction rates of 2-pentene, 2-octene, and 1-phenylpropene on the supported Rh_{2sup} catalyst are similar to each other, whereas the rate enhancements (TOF ratios) for 2-octene and 1-phenylpropene (10 and 7 times, respectively) are much less than that for 2-pentene (51 times). Because length of the linear alkene chains can not be discerned by the ligand-coordinated metal

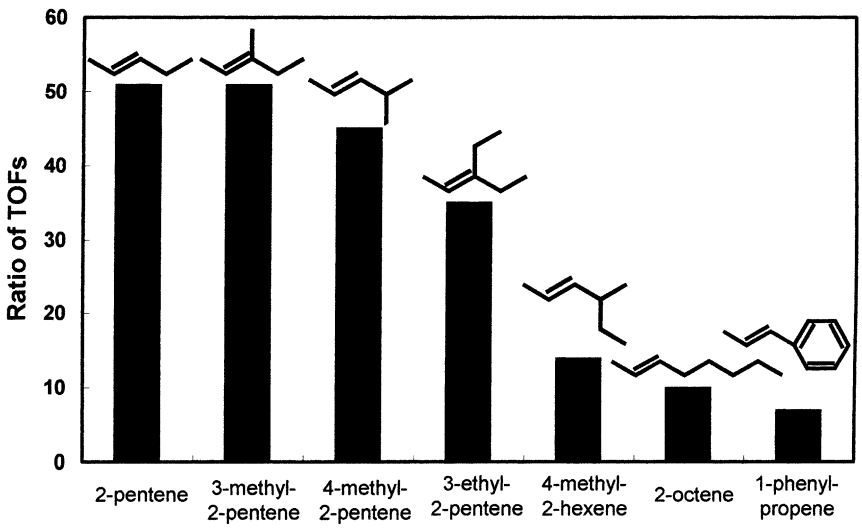

Fig. 18. Degrees of the enhancement of the reaction rates on the Rh-dimer catalyst by the molecular imprinting. Ratio of TOFs: TOF of the imprinted (Rh_{2imp}) Rh-dimer catalyst to TOF of the supported (Rh_{2sup}) catalyst for each alkene.

Table 11
Degrees of enhancement of the reaction rates by molecular imprinting (ratio of TOFs), activation energies (E_a), activation enthalpies ($\Delta^{\ddagger}H$), and activation entropies ($\Delta^{\ddagger}S$) for the catalytic hydrogenation of alkenes at 348 K

Reactant	Ratio of TOFs[a]	Supported catalyst (Rh_{2sup})			Imprinted catalyst (Rh_{2imp})		
		E_a[b]	$\Delta^{\ddagger}H$[c]	$\Delta^{\ddagger}S$[d]	E_a[b]	$\Delta^{\ddagger}H$[c]	$\Delta^{\ddagger}S$[d]
2-Pentene	51	34	31	−205	26	23	−195
3-Methyl-2-pentene	51	44	41	−200	43	40	−170
4-Methyl-2-pentene	45	40	37	−207	40	37	−175
3-Ethyl-2-pentene	35	42	39	−210	39	36	−189
4-Methyl-2-hexene	14	40	37	−212	10	7	−276
2-Octene	10	28	25	−215	7	4	−257
1-Phenylpropene	7	29	26	−213	8	5	−256

[a] Ratio of TOFs: TOF of the Rh_{2imp} catalyst/TOF of the Rh_{2sup} catalyst.
[b] E_a: kJ mol^{-1}.
[c] $\Delta^{\ddagger}H$: kJ mol^{-1}.
[d] $\Delta^{\ddagger}S$: J K^{-1} mol^{-1}.

site, it is suggested that the difference is caused by wall of the template cavity around the Rh dimer site.

Activation energies for the hydrogenation on the Rh_{2sup} catalyst are divided into two values, about 30 and 42 kJ mol^{-1}, for the linear alkenes and the branch alkenes, respectively, in Table 11. Such a large difference in the activation energy has also been observed with the Wilkinson complex. On the contrary, activation entropies for the hydrogenation on the Rh_{2sup} catalyst are similar to each other, which values are in the range −200 to −215 J mol^{-1} K^{-1} for all the alkenes.

After the imprinting, significant differences between small and large alkenes is observed in both activation energies and activation entropies. The activation energies for the hydrogenation of 3-ethyl-2-pentene and smaller alkenes (left four alkenes in Fig. 18) on the imprinted Rh_{2imp} catalyst are 26–43 kJ mol^{-1}, which are similar to the values observed on the Rh_{2sup} catalyst. The activation entropies for the four alkenes are −170 to −195 J mol^{-1} K^{-1}, which are larger than those (−200 to −210 J mol^{-1} K^{-1}) obtained for the Rh_{sup} catalyst. In contrast, for the larger alkenes such as 4-methyl-2-hexene, 2-octene, and 1-phenylpropene, the activation energies are 10, 7, and 8 kJ mol^{-1}, respectively, which are so small compared with those for the Rh_{2sup} catalyst and other metal complex catalysts. Furthermore, the activation entropies reduce prominently from about −210 to about −260 J mol^{-1} K^{-1}. The conspicuous change in the kinetic parameters for the larger alkenes is paralleled to the change in enhancement of the reaction rates. These dramatic decreases in the activation energy and the TOF ratio can be explained by shift of the rate-determining step from the alkyl formation to the coordination of alkene to the Rh site as discussed in Section 8.2. Attended to this shift, the activation entropies for the larger alkene molecules also decreased largely to about −260 from about −180 J mol^{-1} K^{-1} for the other small molecules. It suggests that conformation of the coordinated alkene in the template cavity is regulated by wall of the cavity and remaining $P(OCH_3)_3$ ligands. For the alkenes with the larger sizes and different shapes compared to the template, the coordination to the Rh site through the cavity space becomes most slow in the reaction sequences. The location of Rh center to which the alkenes coordinate, the conformation of remaining $P(OCH_3)_3$ ligand, the orientation of template vacant site on Rh, the template cavity shape, the architecture of the cavity wall, and the micropore surrounding the Rh monomer in the SiO_2-matrix overlayers provide the active Rh_{2imp} catalyst for size- and shape-selective hydrogenation of the alkenes.

Regulation of simple alkenes without any functional groups is in general difficult. The method combining metal-complex attaching and molecular imprinting on the surface demonstrates that the strategy can regulate and design chemical reactions at a molecular level like artificial enzyme catalysts. To our knowledge, the imprinted Rh catalysts are the first example of molecular imprinting of active metal complexes at oxide surfaces. However, achievement of more strict

recognition of molecules needs further investigation and molecular recognition of reactants with functional groups is a next stage of the study. Further, the way may also provide new catalytic systems with tremendous performances for reactions for which enzymes can not be efficient at all and under reaction conditions where enzyme systems can not be applied.

9. Summary

Unique catalytic behaviors of metal complexes different from metal and metal oxides have been devoted to various processes including asymmetric syntheses. Attaching metal complexes on oxide surfaces provides new catalytic systems with advantageous of both heterogeneous and homogeneous catalysts. Combination of the metal-complex attaching with molecular imprinting on oxide surfaces can design advanced catalytic materials, which discriminate methyl and ethyl groups of alkenes without any functional groups. Achievement of more strict recognition of molecules needs further investigation. Nevertheless, the imprinted metal-complex catalysts may be a promising way to deign artificial enzymatic catalysts with 100% selectivity for target reactions.

Acknowledgements

This study was supported by a Grant-in-aid for The 21st Century COE Program for Frontiers in Fundamental Chemistry from the Ministry of Education, Culture, Sports, Science and Technology.

References

[1] J.A. Osborn, F.H. Jardine, J.F. Young, G. Wilkinson, J. Chem. Soc. (A) (1966) 1711.
[2] Y. Iwasawa, Tailored Metal Catalysts, D. Reidel, Dordrecht, 1986.
[3] Y. Iwasawa, Adv. Catal. 87 (1987) 187.
[4] Y. Iwasawa, Catal. Today 18 (1993) 21.
[5] Y. Iwasawa, in: Proceedings of the 11th Congress on Catalysis, Baltimore, Stud. Surf. Sci. Catal. 101 (1996) 21.
[6] Y. Iwasawa, Acc. Chem. Res. 30 (1997) 103.
[7] F.R. Hartley, Supported Metal Complexes, D. Reidel, Dordrecht, 1985.
[8] R. Psaro, S. Recchia, Catal. Today 41 (1–3) (1998) 139.
[9] B.C. Gates, Top. Catal. 14 (1–4) (2001) 173.
[10] A. Zecchina, C.O. Arean, Catal. Rev. Sci. Eng. 35 (1993) 261.
[11] C. Bianchini, P. Frediani, V. Sernau, Organometallics 14 (1995) 5458.
[12] C. Bianchini, A. Meli, V. Patinec, V. Sernau, F. Vizza, J. Am. Chem. Soc. 117 (1997) 4945.
[13] C. Bianchini, D.G. Burnaby, J. Evans, P. Frediani, A. Meli, W. Oberhauser, R. Psaro, L. Sordelli, F. Vizza, J. Am. Chem. Soc. 121 (1999) 5961.
[14] C. Bianchini, E. Farnetti, M. Graziani, J. Kaspar, F. Vizza, J. Am. Chem. Soc. 115 (1993) 1753.
[15] K.K. Bando, K. Asakura, H. Arakawa, K. Isobe, Y. Iwasawa, J. Phys. Chem. 100 (1996) 13636.
[16] K. Asakura, K.K. Bando, Y. Iwasawa, H. Arakawa, K. Isobe, J. Am. Chem. Soc. 112 (1990) 9096.
[17] M. Nishimura, K. Asakura, Y. Iwasawa, J. Chem. Soc., Chem. Commun. (1986) 1660.
[18] N. Ichikuni, K. Asakura, Y. Iwasawa, J. Chem. Soc., Chem. Commun. (1991) 112.
[19] T. Shido, A. Yamaguchi, K. Asakura, Y. Iwasawa, J. Mol. Catal. A: Chem. 163 (2000) 2062.
[20] J.M. Jehng, I.E. Wachs, J. Phys. Chem. 95 (1991) 7373.
[21] Y. Izumi, H. Chihara, H. Yamazaki, Y. Iwasawa, J. Phys. Chem. 98 (1994) 594.
[22] J.D. Grunwaldt, P. Kappen, L. Basini, B.S. Clausen, Catal. Lett. 78 (2002) 13.
[23] A. Zhao, B.C. Gates, Langmuir 13 (1997) 4024.
[24] O. Alexeev, G. Panjabi, B.C. Gates, J. Catal. 173 (1998) 196.
[25] A.M. Argo, J.F. Goellner, B.L. Phillips, G.A. Panjabi, B.C. Gates, J. Am. Chem. Soc. 123 (2001) 2275.
[26] A.M. Argo, J.F. Odzak, F.S. Lai, B.C. Gates, Nature 415 (2002) 623.
[27] B.E. Bent, C.M. Mate, J.E. Crowell, B.E. Koel, G.A. Somorjai, J. Phys. Chem. 91 (1987) 1493.
[28] C.C. Romao, F.E. Kuhn, W.A. Herrmann, Chem. Rev. 97 (1997) 3197.
[29] J. Okal, J. Baran, J. Catal. 203 (2001) 466.
[30] D. Mandelli, M.C.A. van Vliet, U. Arnold, R.A. Sheldon, U. Schuchardt, J. Mol. Catal. A: Chem. 168 (2001) 165.
[31] Y. Yuan, T. Shido, Y. Iwasawa, Chem. Comm. (2000) 1421.
[32] Y. Yuan, Y. Iwasawa, J. Phys. Chem. B 106 (2002) 4441.
[33] N. Viswanadham, T. Shido, Y. Iwasawa, Appl. Catal. A Gen. 219 (2001) 223.
[34] N. Viswanadham, T. Shido, T. Sasaki, Y. Iwasawa, J. Phys. Chem. B 106 (2002) 10955.
[35] D. Meunier, A. Piechaczyk, A. de Mallmann, J.M. Basset, Angew. Chem. Int. Ed. 38 (1999) 3540.
[36] V. Dufaud, G.P. Niccolai, J. Thivolle-Cazat, J.M. Basset, J. Am. Chem. Soc. 117 (1995) 15.
[37] Y. Gao, R.M. Hanson, J.M. Klunder, S.Y. Ko, H. Masumune, K.B. Sharpless, J. Am. Chem. Soc. 109 (1987) 5765.
[38] M.G. Finn, K.B. Sharpless, J. Am. Chem. Soc. 113 (1991) 113.
[39] A. Corma, H. Garcia, A. Moussaif, M.J. Sabater, R. Zniber, A. Redouane, Chem. Commun. (2002) 1058.
[40] P.A. Brady, J.K.M. Sanders, Chem. Soc. Rev. 26 (1997) 327.

[41] D.C. Sherrington, Chem. Commun. (1998) 2275.
[42] M.E. Davis, A. Katz, W.R. Ahmad, Chem. Mater. 8 (1996) 1820.
[43] B. Shellergren, Angew. Chem. Int. Ed. 39 (2000) 1031.
[44] M.J. Whitecombe, C. Alexander, E.N. Vulfson, Synlett 6 (2000) 911.
[45] K. Mosbach, Chem. Rev. 100 (2000) 2495.
[46] M. Tada, Y. Iwasawa, J. Mol. Catal. A: Chem. 199 (2003) 115.
[47] K. Morihara, M. Kurosawa, Y. Kamata, T. Shimada, J. Chem. Soc., Chem. Commun. (1992) 358.
[48] J. Heilmann, W.F. Maier, Angew. Chem. Int. Ed. Engl. 33 (1994) 471.
[49] A. Katz, M.E. Davis, Nature 403 (2000) 286.
[50] A.G. Strikovsky, D. Kasper, M. Crun, B.S. Green, J. Hradil, G. Wulff, J. Am. Chem. Soc. 121 (1999) 6640.
[51] M.A. Markowitz, P.R. Kust, G. Deng, P.E. Schoen, J.S. Dordick, D.S. Clark, B.P. Gaber, Langmuir 16 (2000) 1759.
[52] T. Tanimura, N. Katada, M. Niwa, Langmuir 16 (2000) 3858.
[53] A. Suzuki, M. Tada, T. Sasaki, T. Shido, Y. Iwasawa, J. Mol. Catal. A: Chem. 182–183 (2002) 125.
[54] Y. Fujii, K. Matsutani, K. Kikuchi, J. Chem. Soc., Chem. Commun. (1985) 415.
[55] J. Suh, Y. Cho, K.J. Lee, J. Am. Chem. Soc. 113 (1991) 4198.
[56] J.F. Krebs, A.S. Borovik, J. Am. Chem. Soc. 117 (1995) 10593.
[57] J.F. Krebs, A.S. Borovik, Chem. Commun. (1998) 553.
[58] N.M. Brunkan, M.R. Gagne, J. Am. Chem. Soc. 122 (2000) 6217.
[59] J. Matsui, I.A. Nicholls, I. Karube, K. Mosbach, J. Org. Chem. 61 (1996) 5414.
[60] F. Locatelli, P. Gamez, M. Lemaire, J. Mol. Catal. A: Chem. 135 (1998) 89.
[61] B.P. Santora, A.O. Larsen, M.R. Gagne, Organometallics 17 (1998) 3138.
[62] K. Polborn, K. Severin, Chem. Eur. J. 6 (2000) 4604.
[63] K. Polborn, K. Severin, Eur. J. Inorg. Chem. (2000) 1687.
[64] A.N. Cammidge, N.J. Baines, R.K. Bellingham, Chem. Commun. (2001) 2588.
[65] M. Tada, T. Sasaki, Y. Iwasawa, Phys. Chem. Chem. Phys. 4 (2002) 4561.
[66] M. Tada, T. Sasaki, T. Shido, Y. Iwasawa, Phys. Chem. Chem. Phys. 4 (2002) 5899.
[67] M. Tada, T. Sasaki, Y. Iwasawa, J. Catal. 211 (2002) 496.